Parameter space geometry of the quartic oscillator and the double-well potential: classical and quantum description

Physica Scripta

PAPER

Parameter space geometry of the quartic oscillator and the double-well potential: classical and quantum description

Diego Gonzalez[1,2], **Jorge Chávez-Carlos**[3], **Jorge G Hirsch**[4] and **J David Vergara**[4,*]

[1] Escuela Superior de Ingeniería Mecánica y Eléctrica, Instituto Politécnico Nacional, 07738 Ciudad de México, Mexico
[2] Departamento de Física, Cinvestav, Avenida Instituto Politécnico Nacional 2508, San Pedro Zacatenco, 07360 Gustavo A. Madero, Ciudad de México, Mexico
[3] Department of Physics, University of Connecticut, Storrs, Connecticut 06269, United States of America
[4] Instituto de Ciencias Nucleares, Universidad Nacional Autónoma de México, Apartado Postal 70-543, Ciudad de México, 04510, Mexico
[*] Author to whom any correspondence should be addressed.

E-mail: dgonzalezv@ipn.mx, jorge.chavez_carlos@uconn.edu, hirsch@nucleares.unam.mx and vergara@nucleares.unam.mx

Keywords: geometry, anharmonic oscillator, quantum metric tensor, semiclassical formalism, quantum phase transition

OPEN ACCESS

RECEIVED
15 September 2023

REVISED
10 January 2024

ACCEPTED FOR PUBLICATION
12 January 2024

PUBLISHED
25 January 2024

Abstract

We compute the quantum metric tensor and its scalar curvature for the anharmonic oscillator for positive and negative quadratic potentials, where the potential displays a double well, employing exact numerical and perturbative procedures. We also introduce a formulation of the classical analog of the quantum metric tensor by using a novel approach based on Fourier series, which is shown to reproduce the relevant quantum features involved in the parameter space. It is remarkable that both the exact quantum treatment and classical formalism recognize the negative oscillator parameter at which the ground state starts to be delocalized in two wells.

1. Introduction

Exploring the quantum parameter space's geometry has led to captivating insights into various physical systems [1–5]. Within these investigations, a prominent element is the quantum geometric tensor (QGT), encompassing the quantum metric tensor (QMT) in its real part and the Berry curvature in its imaginary part. This tensor holds significance in quantum information processing applications, such as adiabatic and holonomic quantum computing [6]. In these applications, minimizing errors corresponds to traversing geodesics on the control parameter manifold [7]. The QGT plays a vital role in describing quantum phase transitions (QPT) in the thermodynamic limit and provides valuable information about the precursors to these transitions when dealing with systems comprising a finite number of particles. Furthermore, following the ideas of Ozawa and Goldman [8, 9], recently has been possible to measure the QMT experimentally [10, 11], showing that the QGT can be a relevant tool to describe quantum phenomena as, for example, the observations of the quantum geometry that enabled an evaluation of the quantum Cramér-Rao bound (QCRB) [12, 13].

In this study, we extensively examine the geometry of the quantum parameter space for the anharmonic oscillator. To our knowledge, a systematic investigation of the geometric properties of the quantum parameter space of the anharmonic oscillator has not been undertaken. Therefore, one objective of this article is to fill this gap by conducting a thorough analysis of the quantum geometric tensor of this system.

To do this, we introduced a notion of distance in this space using the quantum metric tensor developed by Provost *et al* [1] and Zanardi *et al* [2]. With the help of this metric, we can reconstruct all the geometric information of the parameter space, including the scalar curvature, which shows quite interesting behaviors for both positive and negative oscillator parameters.

We employ two techniques to construct the quantum metric tensor for the ground state of the anharmonic oscillator, which has a double-well potential in the case of negative oscillator parameters. We obtain an exact numerical description performing a diagonalization in a truncated harmonic oscillator basis [14], including a careful analysis of the convergence of all the relevant observables, along with the perturbative method outlined by Zanardi *et al* [2]. These numerical results are compared with a perturbative procedure of nonlinearization to

express the wave function as a power series in λ [15], and with a novel classical procedure employing Fourier series. This particular approach involves constructing a classical analog of the quantum metric tensor [16], offering the advantage of enabling the derivation of the classical equivalent of the matrix element of an operator between the ground state and any excited state.

The most important results of this work are that the classical analog of the quantum metric tensor reproduces the relevant quantum features involved in the parameter space and that both the exact quantum treatment and classical formalism recognize the negative oscillator parameter at which the ground state starts to be delocalized in two wells.

The structure of the article is as follows: in section 2 we introduce the Quantum metric tensor (QMT) and its classical version, in section 3 the quartic oscillator Hamiltonian is presented, including the calculation of the QMT employing the exact numerical quantum analysis, the quantum perturbative approach and the classical formalism. A detailed comparison between the exact and perturbative quantum metrics is presented in section 4, and between quantum and classical approaches in section 5. Section 6 contains the conclusions. In the appendices tables and plots are presented, which would help the reader interested in reproducing the calculations and to follow in detail how the comparisons are performed and at which level the different formalisms provide similar results.

2. Geometry of the parameter space

In this section, we introduce some basic aspects involved in parameter space associated with quantum and classical systems, as well as fix some notations.

2.1. Quantum metric tensor

We start by considering a one-dimensional quantum system with a Hamiltonian $\hat{H}(\hat{q},\,\hat{p};\,x)$ that depends on a set of $\mathfrak{m}$ real adiabatic parameters denoted by $x = \{x^i\}$ $(i = 1,\ldots,\mathfrak{m})$. It is assumed that the Hamiltonian has at least one eigenvector $|\Psi_n(x)\rangle$ with nondegenerate eigenvalue $E_n(x)$. Using this eigenvector, the components of the quantum metric tensor (QMT) defined in the m-dimensional parameter space $\mathcal{M}$ of the system are given by [1]

$$g_{ij}^{(n)} \coloneqq \mathrm{Re}(\langle\partial_i\Psi_n|\partial_j\Psi_n\rangle - \langle\partial_i\Psi_n|\Psi_n\rangle\langle\Psi_n|\partial_j\Psi_n\rangle), \tag{1}$$

where $\partial_i \coloneqq \frac{\partial}{\partial x^i}$. This metric provides the distance between the eigenvectors $|\Psi_n(x)\rangle$ and $|\Psi_n(x+\delta x)\rangle$ with infinitesimally different parameters, namely $\delta\ell^2 = g_{ij}^{(n)}(x)\delta x^i\delta x^j$. For the purposes of this work, it is convenient to introduce the perturbative form of this metric [2]

$$g_{ij}^{(n)} = \mathrm{Re}\sum_{m\neq n}\frac{\langle\Psi_n|\hat{O}_i|\Psi_m\rangle\langle\Psi_m|\hat{O}_j|\Psi_n\rangle}{(E_m - E_n)^2}, \tag{2}$$

where we introduced the operators $\hat{O}_i \equiv \partial_i\hat{H}$. Notice that to evaluate the expression (2) all the matrix elements must be known. The advantage of this expression is that it shows that the components of the QMT are singular at the points $x^* \in \mathcal{M}$ of the parameter space such that $E_m(x^*) = E_n(x^*)$. This means that at the critical points of the QPT, the components of the QMT are singular. However, in some cases, a more detailed analysis is required [5, 17].

For the purposes of this study, we set $n = 0$ and write the QMT (2) as

$$g_{ij}^{(0)} = \mathrm{Re}\sum_{m=1}^{\infty} G_{ij}^{(m)}, \tag{3}$$

with

$$G_{ij}^{(m)} \coloneqq \frac{B_i^{(m)}(B_j^{(m)})^*}{(E_m - E_0)^2}, \tag{4}$$

where $*$ denotes the complex conjugate, and we have defined the transition matrix elements $B_i^{(m)} \coloneqq \langle\Psi_0|\partial_i\hat{H}|\Psi_m\rangle$, that in the context of non-adiabatic molecular mechanics are known as the non-adiabatic coupling vectors [18, 19].

To find out whether the resulting singularities are genuine or merely a result of the parameter space's coordinates, we can resort to the scalar curvature R, which does not depend on the coordinates used.

In particular, for a two-dimensional space endowed with a metric tensor (the QMT, in this case), the scalar curvature has the simple form [20]

$$R = \frac{1}{\sqrt{|g|}}(\mathcal{A} + \mathcal{B}), \tag{5}$$

where $g = \det[g_{ij}]$ is the determinant of the metric and the quantities $\mathcal{A}$ and $\mathcal{B}$ are defined as

$$\begin{aligned}\mathcal{A} &:= \partial_1\left(\frac{g_{12}}{g_{11}\sqrt{|g|}}\partial_2 g_{11} - \frac{1}{\sqrt{|g|}}\partial_1 g_{22}\right),\\ \mathcal{B} &:= \partial_2\left(\frac{2}{\sqrt{|g|}}\partial_1 g_{12} - \frac{1}{\sqrt{|g|}}\partial_2 g_{11} - \frac{g_{12}}{g_{11}\sqrt{|g|}}\partial_1 g_{11}\right).\end{aligned} \tag{6}$$

2.2. Classical metric tensor

Let us now consider a one-dimensional classical integrable system described by a Hamiltonian $H(q,\ p;\ x)$ depending on the set of real adiabatic parameters $x = \{x^i\}$ $(i = 1, \ldots, \mathfrak{m})$. The natural coordinates for this type of systems are the action-angle variables $\{I, \phi\}$, which allow to write the Hamiltonian as $H(I;\ x) = H(q(\phi,\ I;\ x),\ p(\phi,\ I;\ x);\ x)$ and can be used to define the torus average of a function $f(I,\ \phi;\ x)$ as

$$\langle f(\phi,\ I;\ x)\rangle = \frac{1}{(2\pi)^N}\int_0^{2\pi} \mathrm{d}^N\phi\, f(\phi,\ I;\ x). \tag{7}$$

In this setting, the classical analog of the quantum metric tensor (1) is [21, 22]

$$g_{ij}(I;\ x) = -\int_{-\infty}^{0} \mathrm{d}t_1 \int_0^{\infty} \mathrm{d}t_2(\langle \mathcal{O}_i(t_1)\,\mathcal{O}_j(t_2)\rangle_0 - \langle \mathcal{O}_i(t_1)\rangle_0\langle \mathcal{O}_j(t_2)\rangle_0), \tag{8}$$

where $\langle\cdot\rangle_0$ means that the classical average (7) is taken over the initial $(t = 0)$ angle variable ϕ_0 and $\mathcal{O}_i(t)$ are $\mathfrak{m}$ time-dependent functions defined as

$$\mathcal{O}_i(t) \equiv \mathcal{O}_i(q(t),\ p(t);\ x) = (\partial_i H)_{q,p}. \tag{9}$$

This classical metric tensor (CMT) provides a measure of the distance, on the parameter space $\mathcal{M}$, between the points $[q(x),\ p(x)]$ and $[q(x + \delta x),\ p(x + \delta x)]$ with infinitesimally different parameters, i.e., $\delta\ell^2 = g_{ij}(I;\ x)\delta x^i\delta x^j$.

Since the functions $\mathcal{O}_i(t)$ are periodic in the angle variable ϕ, they can be expressed as a Fourier series as

$$\mathcal{O}_i(t) = \sum_{m'=-\infty}^{\infty} \beta_i^{(m')}\mathrm{e}^{\mathrm{i}m'\phi(t)}, \tag{10}$$

where $\phi(t) = \phi_0 + \omega t$ with $\omega = \partial H/\partial I$ the angular frequency of the system, 'i' is the imaginary unit, and $\beta_i^{(m')}$ are the time-independent Fourier coefficients

$$\beta_i^{(m')}(I;\ x) \equiv \langle \mathcal{O}_i(\phi,\ I;\ x)\mathrm{e}^{-\mathrm{i}m'\phi}\rangle. \tag{11}$$

Using the functions $\beta_i^{(m')}$, it can be shown that the components of CMT (8) can be equivalently written as [23]

$$g_{ij}(I;\ x) = \sum_{\substack{m'=-\infty\\ m'\neq 0}}^{\infty} \frac{\beta_i^{(m')}\,\beta_j^{(-m')}}{(m'\omega)^2}. \tag{12}$$

This expression can be regarded as the perturbative form of the CMT, and in this sense, it is analogous to the expression (2) of the QMT. The appealing feature of (12) is that it does not require solving the initial conditions problem, which makes it suitable for this study. To determine if the resulting singularities of this metric are genuine or not, we can also compute the associate scalar curvature (5) of the two-dimensional case.

Notice that the CMT (12) can be written in a similar fashion as the QMT (3). In fact, using $(\beta_i^{(m')})^* = \beta_i^{(-m')}$ which follows from (11), the CMT can be expressed as

$$g_{ij}(I;\ x) = \mathrm{Re}\sum_{m'=1}^{\infty} \mathcal{G}_{ij}^{(m')}, \tag{13}$$

with

$$\mathcal{G}_{ij}^{(m')} := \frac{\beta_i'^{(m')}\,(\beta_j'^{(m')})^*}{(m\omega)^2}, \tag{14}$$

where we have defined $\beta_i'^{(m')} := \sqrt{2}\,\beta_i^{(m')}$. In this way, we can recognize the classical analog of the quantum non-adiabatic coupling vectors $B_i^{(m)}$, which are our classical functions $\beta_i'^{(m')}$. In section 5, we will perform a direct comparison of the quantum calculations and their classical analogs.

3. Quartic oscillator and double well potential

The Hamiltonian of the quantum quartic oscillator is

$$\hat{H} = \frac{1}{2}\hat{p}^2 + \frac{k}{2}\hat{q}^2 + \frac{\lambda}{4!}\hat{q}^4, \tag{15}$$

where k and λ are the system parameters, which we adopt as our adiabatic parameters. Then, the associated parameter space corresponds to a two-dimensional manifold with coordinates $\{x^i\} = (k,\ \lambda), i = 1,2$. Throughout this paper, we consider $\lambda > 0$. In the case $k > 0$, the potential has a single minimum, while in the case $k < 0$ it has two minima and is known as the double-well potential.

The anharmonic oscillator is a system that has been analyzed from many points of view. In the original articles by Bender and Wu [24, 25], it was shown that, using semiclassical methods of WKB, the large $n-$ behavior in the series expansion of the energy levels of the perturbation calculus is divergent. Later, this study was followed by the perturbative analysis of Lipatov [26] and Brézin *et al* [27], showing that the presence of the instanton connecting the two minima of the potential is responsible for the non-Borel summability of the perturbation expansion of the ground state energy. The anharmonic oscillator has served as a test system, useful to extend the results to quantum field theory, and its large order behavior has been analyzed using instanton contributions to the path integral representation of Green's functions [28–31]. These studies were extended considering the contributions of multi-instantons to the ground state in [32] and to excited states in [33].

In [34], it was shown that a summable perturbation series exists for the double-well potential employing an effective coupling. Subsequently, in [35] a fast convergence in perturbation theory was introduced using a simple uniform approximation of the logarithmic derivative of the ground state eigenfunction. This technique transforms the one-dimensional Schrödinger equation into a Riccati form, using the logarithmic derivative of the wave function [36]. Using this approach, in [37] approximate eigenfunctions were obtained for the quartic anharmonic oscillator, and also for the double-well potential [38, 39].

3.1. Quantum analysis

3.1.1. QMT from a numerical calculation

The quantum Hamiltonian (15) is easily represented with the creation and annihilation operators considering the following equations,

$$\hat{q} = \sqrt{\frac{\hbar}{2m\omega}}(\hat{a} + \hat{a}^\dagger), \quad \hat{p} = -i\sqrt{\frac{m\omega\hbar}{2}}(\hat{a} - \hat{a}^\dagger), \tag{16}$$

where $\omega = \sqrt{k/m}$. Consequently, the Hamiltonian becomes,

$$\hat{H} = \tfrac{\hbar\omega}{2}(1 + 2\hat{a}^\dagger\hat{a}) + \tfrac{\hbar\lambda}{4\cdot 4! m^2\omega^2}(\hat{a}^\dagger + \hat{a})^4, \tag{17}$$

the respective matrix elements of $\hat{H}$ can be represented in the Fock basis and are given by,

$$\begin{aligned}\langle n'|\hat{H}|n\rangle = &\left[\left(\tfrac{\omega\hbar}{2}\right)(1 + 2n) + \left(\tfrac{\lambda\hbar^2}{96m^2\omega^2}\right)(6n^2 + 6n + 3)\right]\delta_{n',n} \\ &+ \sqrt{(n+1)(n+2)}\,[(4n+6)\,\delta_{n',n+2} \\ &+ \sqrt{(n+1)(n+2)(n+3)(n+4)}\,\delta_{n',n+4}]\left(\tfrac{\lambda\hbar^2}{96m^2\omega^2}\right) + \text{c.c.}\end{aligned} \tag{18}$$

With these matrix elements, a truncated Hamiltonian matrix is built with $n,\ n' \in [0,\ N]$, where N is the finite truncated size on the Fock basis, which allows to obtain N_{conv} converged eigenstates. We encode in Mathematica [40] the calculations to find the first N_{conv} eigenstates $|\Psi_m\rangle$ of the system, preserving a numerical accuracy of seventy digits of precision.

Using (15), for k and λ we get

$$\hat{O}_1 \equiv \frac{\partial\hat{H}}{\partial k} = \frac{\hat{q}^2}{2}, \tag{19a}$$

$$\hat{O}_2 \equiv \frac{\partial\hat{H}}{\partial\lambda} = \frac{\hat{q}^4}{4!}. \tag{19b}$$

Both quantities are substituted into (2). The cutoff N_{conv} guarantees that the transition matrix elements of $\hat{O}_1$ and $\hat{O}_2$ converged. Having obtained numerically the eigenstates, energies, and the transition operators $\hat{O}_1$ and $\hat{O}_2$ we calculate numerically the elements of the QMT g_{ij} point by point in the bidimensional parameter space. Employing the command `Interpolation[...,Method->Hermite]` defined in Mathematica, g_{ij} is represented as a continuous, differentiable function. In this way we can use the analytical expression (5) and obtain the Ricci scalar R.

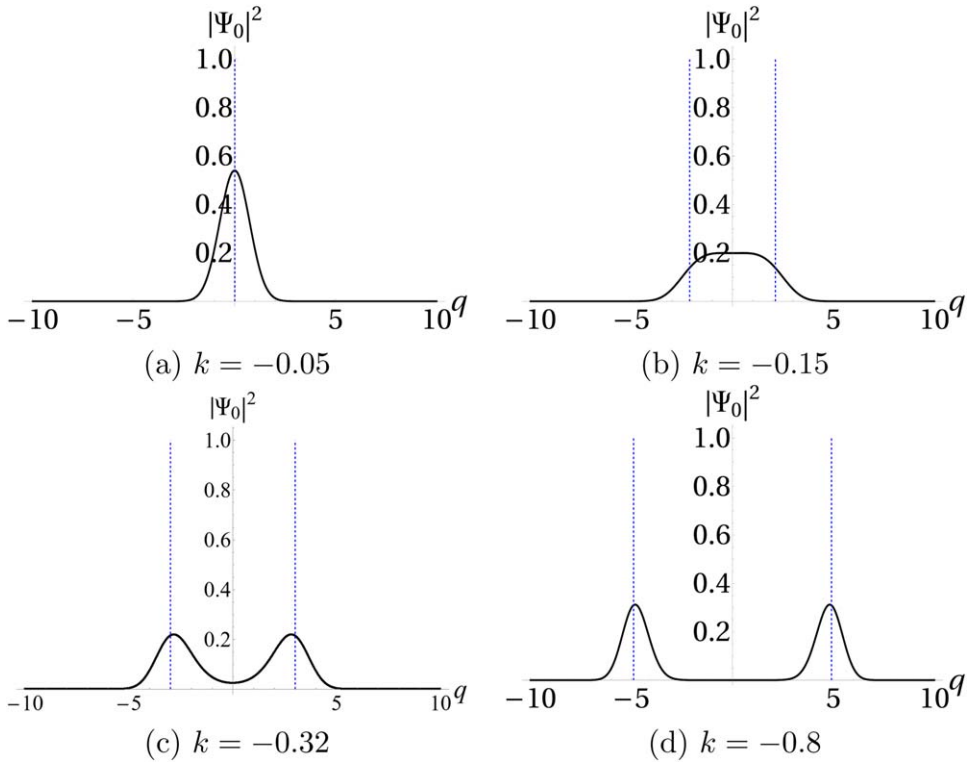

Figure 1. $|\Psi_0(q)|^2$ for $\lambda = 0.2$. Dashed blue lines are the position for the classical critical point.

The classical limit of the Hamiltonian (15) has a double well potential if $k < 0$ and a simple well if $k > 0$. To visualize the behaviour in the q variable for the quantum system, we employ the ground state $|\Psi_0\rangle$ expanded in the quantum harmonic oscillator basis $|\Phi_l\rangle$, so,

$$\Psi_0(q) \equiv \langle q|\Psi_0\rangle = \sum_l C_{0,l}\langle q|\Phi_l\rangle, \tag{20}$$

where the coefficients $C_{0,l} = \langle\Phi_l|\Psi_0\rangle$ are obtained in the numerical diagonalization and

$$\langle q|\Phi_l\rangle = \frac{1}{\sqrt{2^l l!}}\left(\frac{m\omega}{\pi\hbar}\right)^{1/4}\exp\left(\frac{-m\omega q^2}{2\hbar}\right)H_l(\sqrt{m\omega/\hbar}q), \tag{21}$$

with H_l the Hermite polynomial of l-degree.

The ground state probability distribution $|\Psi_0(q)|^2$ to find the particle at the position q has a maximum at $q = 0$ for $k > 0$. For $k < 0$, it shows an interesting behavior, displayed in figure 1. It has one maximum for small values of $|k|$ and, for $\lambda = 0.2$, it starts noticing the presence of the two wells at $k \approx -0.15$ and develops two separated probability regions at $k \approx -0.32$. The delocalization of the probability distribution over the two wells occurs when the ground state energy is lower than the top of the energy barrier between the two wells. This effect can be best visualized in figure 2, where the blue lines represent the position of the minima of the classical potential, the yellow bands the exact quantum ground state probability distribution, with their maxima depicted with red dots.

3.1.2. QMT from a perturbative approach

Here we consider a perturbative treatment in the parameter λ since there is no exact analytical solution to the resulting Schrödinger equation. Furthermore, we restrict ourselves to obtain the ground-state wave function and its energy up to the 10th order in λ. To accomplish this task, we will use the method proposed in [15], suitable for finding corrections to large powers of λ. The wave function generated by this approach, shown as an example up to the fourth order in λ is

$$\begin{aligned}\Psi_0(q) = e^{-\frac{1}{2}\sqrt{k}q^2} &- \frac{\lambda q^2 e^{-\frac{1}{2}\sqrt{k}q^2}}{96k}P_1 + \frac{\lambda^2 q^2 e^{-\frac{1}{2}\sqrt{k}q^2}}{55296k^{5/2}}P_2 \\ &- \frac{\lambda^3 q^2 e^{-\frac{1}{2}\sqrt{k}q^2}}{5308416k^4}P_3 + \frac{\lambda^4 q^2 e^{-\frac{1}{2}\sqrt{k}q^2}}{6115295232k^{11/2}}P_4 + ...,\end{aligned} \tag{22}$$

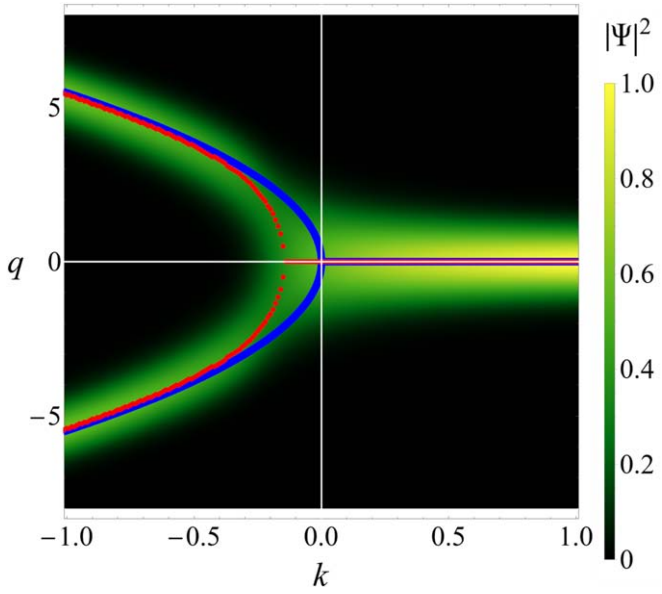

Figure 2. $|\Psi_0(q)|^2$ for $\lambda = 0.2$ in function of q and k, the blue curve is the classical localization of the critical points, and the red curve is the maximal value of $|\Psi(q)|^2$ obtained numerically.

where

$$P_1 = \sqrt{k}q^2 + 3, \tag{23a}$$

$$P_2 = 3k^{3/2}q^6 + 26kq^4 + 93\sqrt{k}q^2 + 252, \tag{23b}$$

$$P_3 = k^{5/2}q^{10} + 141k^{3/2}q^6 + 17k^2q^8 + 813kq^4 + 2916\sqrt{k}q^2 + 7992, \tag{23c}$$

$$P_4 = 3k^{7/2}q^{14} + 1198k^{5/2}q^{10} + 82755k^{3/2}q^6 + 84k^3q^{12} + 11748k^2q^8 + 443064kq^4 + 1599552\sqrt{k}q^2 + 4447440. \tag{23d}$$

Using the wave function up to the tenth order in λ together with the Provost and Valle formula (1), we get the QMT components for $k > 0$

$$g_{11} = \frac{1}{k^2}\sum_{\alpha=0}^{10}(-1)^\alpha a_\alpha^{(11)}\left(\frac{\hbar\lambda}{k^{3/2}}\right)^\alpha, \tag{24a}$$

$$g_{12} = \frac{\hbar}{k^{5/2}}\sum_{\alpha=0}^{10}(-1)^\alpha a_\alpha^{(12)}\left(\frac{\hbar\lambda}{k^{3/2}}\right)^\alpha, \tag{24b}$$

$$g_{22} = \frac{\hbar^2}{k^3}\sum_{\alpha=0}^{10}(-1)^\alpha a_\alpha^{(22)}\left(\frac{\hbar\lambda}{k^{3/2}}\right)^\alpha. \tag{24c}$$

where the coefficients $a_\alpha^{(ij)}$ are given in the table 1. It is evident from the above equations that all the components of the QMT will diverge when $k \to 0$. It is also relevant to mention that the quantum perturbative analysis presented in this subsection can only be performed for $k > 0$.

3.2. Classical analysis

In this section, we consider the classical counterpart of quantum Hamiltonian (15), which is given by

$$H = \frac{1}{2}p^2 + \frac{k}{2}q^2 + \frac{\lambda}{4!}q^4, \tag{25}$$

and also take $\{x^i\} = (k, \lambda)$ with $i = 1, 2$ as the set of adiabatic parameters. The classical metric tensor for this system in the case $k > 0$ was obtained in [21], by using a formulation based on generating functions and resorting to the canonical perturbation theory. However, in [21] neither the scalar curvature associated with the geometry of the parameter space nor the more challenging case of $k < 0$ were studied. The aim of the section is to provide a complete analysis of the parameter space of these systems in both cases, $k > 0$ and $k < 0$, in the framework of the Fourier-base formulation (12).

Table 1. Coefficients of the QMT (24).

α	$a_\alpha^{(11)}[\times 10^{-2}]$	$a_\alpha^{(12)}[\times 10^{-2}]$	$a_\alpha^{(22)}[\times 10^{-2}]$
0	3.125	0.781 25	0.211 59
1	2.1484	0.724 28	0.252 28
2	1.5971	0.651 21	0.269 51
3	1.3201	0.622 12	0.294 84
4	1.2078	0.642 18	0.341 33
5	1.2156	0.718 47	0.422 64
6	1.3384	0.870 78	0.561 67
7	1.6053	1.1413	0.801 55
8	2.0893	1.6137	1.2271
9	2.9401	2.4552	2.0117
10	4.4588	4.0081	3.5236

To compute the classical metric (12), we begin by setting the functions (9). Using (25), for k and λ we get

$$\mathcal{O}_1 \equiv \left(\frac{\partial H}{\partial k}\right)_{q,p} = \frac{q^2}{2}, \tag{26a}$$

$$\mathcal{O}_2 \equiv \left(\frac{\partial H}{\partial \lambda}\right)_{q,p} = \frac{q^4}{4!}. \tag{26b}$$

The next step is to obtain the Fourier coefficients (11), which requires first expressing these deformation functions in terms of the system's action-angle variables $\{I, \phi\}$. Since finding the action-angle variables for the Hamiltonian (25) is not easy, we need to resort to the canonical perturbation theory [41]. We carry this out by separately considering the cases $k > 0$ and $k < 0$. It is essential to point out that functions (26*a*) and (26*b*) hold for both cases.

3.2.1. Case $k > 0$

In the canonical perturbation theory, a problem is solved by decomposing the Hamiltonian into a well understood system plus a perturbation term. Since in this case, we have only a fixed point, shown in figure 3.

The Hamiltonian (25) can be decomposed as $H = H_0 + \lambda H_1$, with

$$H_0 = \frac{1}{2}p^2 + \frac{k}{2}q^2, \tag{27}$$

$$H_1 = \frac{q^4}{4!}. \tag{28}$$

Assuming $\lambda \ll 1$, H_0 can be regarded as the Hamiltonian of the unperturbed problem and has well-known action-angle variables $\{I_0, \phi_0\}$, which are related to the variables $\{q, p\}$ as

$$q(\phi_0, I_0; x) = \left(\frac{2I_0}{\omega_0}\right)^{1/2} \sin\phi_0, \tag{29a}$$

$$p(\phi_0, I_0; x) = (2\omega_0 I_0)^{1/2} \cos\phi_0, \tag{29b}$$

where $\omega_0 = \sqrt{k}$ is the frequency of the unperturbed system. Furthermore, in this setting H_1 is understood as the perturbative potential.

In the perturbation theory, the type 2 generating function $W(\phi_0, I; x)$ of the canonical transformation from (ϕ_0, I_0) to the action-angle variables (ϕ, I) of the total Hamiltonian $H(I; x)$ can be written as

$$W(\phi_0, I; x) = \phi_0 I + \lambda W_1(\phi_0, I; x) + \lambda^2 W_2(\phi_0, I; x)..., \tag{30}$$

where W_1, W_2,... are functions obtained by solving the differential equations [41, 42]

$$\omega_0 \frac{\partial W_\mu(\phi_0, I; x)}{\partial \phi_0} = \langle \Phi_\mu(\phi_0, I; x)\rangle_0 - \Phi_\mu(\phi_0, I; x). \tag{31}$$

Here, $\langle\cdot\rangle_0$ is the classical average with respect to unperturbed angle ϕ_0 and, in particular, the first three functions Φ_μ are obtained by $\Phi_1 = H_1$, $\Phi_2 = \frac{\partial W_1}{\partial \phi_0}\frac{\partial H_1}{\partial I}$ and $\Phi_3 = \frac{1}{2}\left(\frac{\partial W_1}{\partial \phi_0}\right)^2 \frac{\partial^2 H_1}{\partial I^2} + \frac{\partial W_2}{\partial \phi_0}\frac{\partial H_1}{\partial I}$. Using this, we compute the functions W_μ for $\mu = 1,\ldots,10$, which are provided in A (see equation (A.1)).

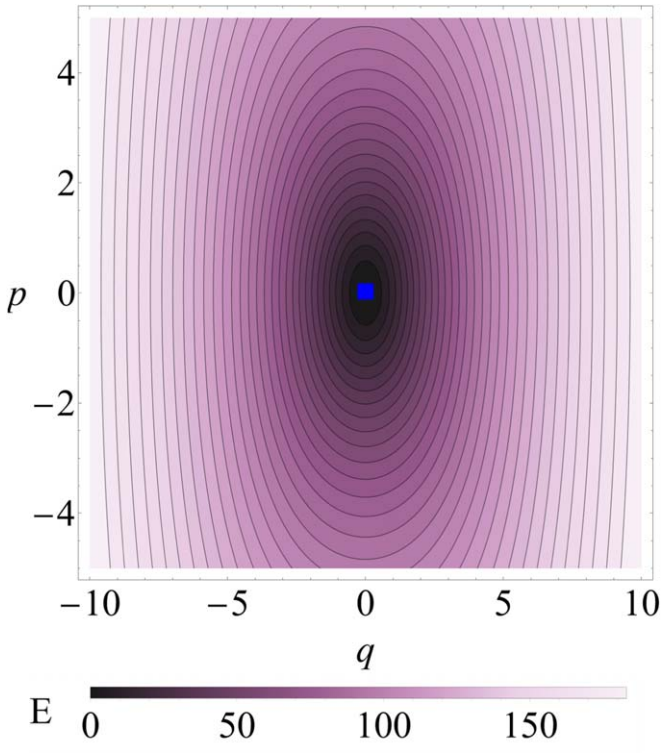

Figure 3. Energy surfaces for $k = 1$ and $\lambda = 0.2$.

With the generating function W at hand and bearing in mind the equations of the canonical transformation

$$\phi(\phi_0, I; x) = \frac{\partial W(\phi_0, I; x)}{\partial I}, \tag{32a}$$

$$I_0(\phi_0, I; x) = \frac{\partial W(\phi_0, I; x)}{\partial \phi_0}, \tag{32b}$$

the variables ϕ and I_0 can be calculated in terms of ϕ_0, I, and the parameters x. Then, using (29*a*) together with the resulting action variable $I_0(\phi_0, I; x)$, the classical deformation functions (26*a*) and (26*b*) can also be expressed in terms of the ϕ_0, I, and x, i.e. $\mathcal{O}_1 = \mathcal{O}_1(\phi_0, I; x)$ and $\mathcal{O}_2 = \mathcal{O}_2(\phi_0, I; x)$ which are given in (A.2) and (A.3) up to the fourth order in λ. Because of this, it is convenient to perform the change of variable $\phi \to \phi_0$ in (11), which allows us to write the expression for the Fourier coefficients as

$$\beta_j^{(n')}(I; x) = \left\langle \frac{\partial \phi(\phi_0, I; x)}{\partial \phi_0} \mathcal{O}_j(\phi_0, I; x) \mathrm{e}^{-\mathrm{i}n'\phi(\phi_0, I; x)} \right\rangle_0. \tag{33}$$

From this expression we obtain the coefficients $\beta_1^{(n')}(I; x)$ and $\beta_2^{(n')}(I; x)$ for $n' = 0, \pm 1, \ldots, \pm 10$, which are given in (A.4) and (A.5), respectively.

Substituting (A.4) and (A.5) into (12), the components of the classical metric tensor for $k > 0$ are

$$g_{11}^{\mathrm{cl}} = \frac{I^2}{k^2} \sum_{\alpha=0}^{10} (-1)^\alpha b_\alpha^{(11)} \left(\frac{I\lambda}{k^{3/2}} \right)^\alpha, \tag{34a}$$

$$g_{12}^{\mathrm{cl}} = \frac{I^3}{k^{5/2}} \sum_{\alpha=0}^{10} (-1)^\alpha b_\alpha^{(12)} \left(\frac{I\lambda}{k^{3/2}} \right)^\alpha, \tag{34b}$$

$$g_{22}^{\mathrm{cl}} = \frac{I^4}{k^3} \sum_{\alpha=0}^{10} (-1)^\alpha b_\alpha^{(22)} \left(\frac{I\lambda}{k^{3/2}} \right)^\alpha, \tag{34c}$$

where the numerical coefficients $b_\alpha^{(11)}$, $b_\alpha^{(12)}$, and $b_\alpha^{(22)}$ are given in table 2. As in the quantum case, all the components of the CMT will also diverge when $k \to 0$.

3.2.2. Case k < 0

In this case, the system presents three fixed points corresponding to vanishing phase space velocities $(\dot{q}, \dot{p})$. The points are

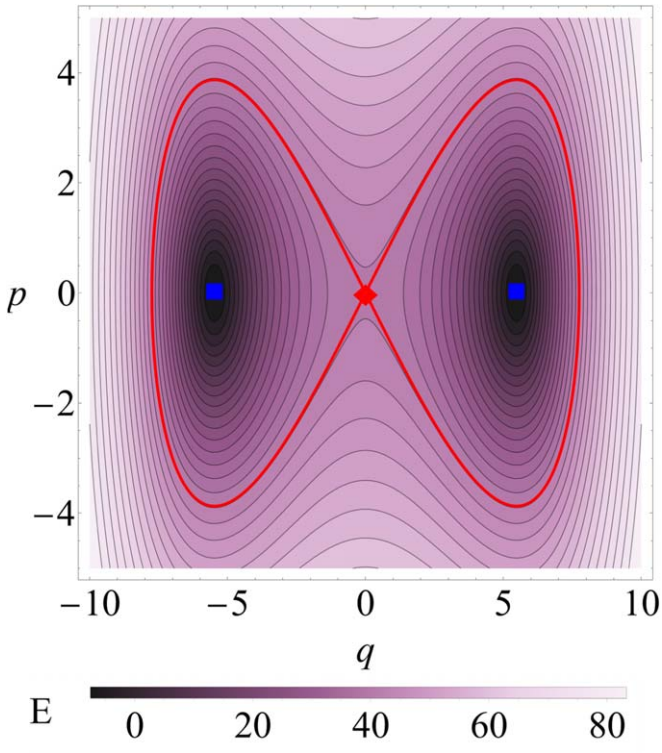

Figure 4. Energy surfaces for $k = -1$ and $\lambda = 0.2$. Blue points are the stable center points χ_1 and χ_3, whereas the red one is the unstable center point χ_2.

Table 2. Coefficients of the classical metric tensor (34).

α	$b_\alpha^{(11)}[\times 10^{-4}]$	$b_\alpha^{(12)}[\times 10^{-4}]$	$b_\alpha^{(22)}[\times 10^{-5}]$
0	312.5	52.083	88.162
1	143.23	29.772	60.357
2	65.07	15.191	34.176
3	30.272	7.6057	18.337
4	14.402	3.8085	9.6513
5	6.9781	1.9169	5.0451
6	3.4315	0.970 81	2.6326
7	1.7079	0.494 72	1.3745
8	0.858 56	0.253 55	0.718 78
9	0.4352	0.130 62	0.376 65
10	0.222 16	0.067 608	0.197 81

$$\chi_1 = (q, p) = \left(-\sqrt{\frac{-6k}{\lambda}}, 0\right), \tag{35a}$$

$$\chi_2 = (q, p) = (0, 0), \tag{35b}$$

$$\chi_3 = (q, p) = \left(\sqrt{\frac{-6k}{\lambda}}, 0\right). \tag{35c}$$

In figure 4, we can see these points. The blue points correspond to χ_1 and χ_3, which are center points as long as $k < 0$. Furthermore, the red point corresponds to χ_2 and it is a hyperbolic point.

Taking into account this, it is convenient to carry out a transformation to a coordinate system centered on χ_1 or χ_3. Then, let us take the point χ_1 and consider the change of coordinates $Q = q + \sqrt{\frac{-6k}{\lambda}}$ and $P = p$. In terms of the new variables the Hamiltonian (25) reads

$$H = \frac{1}{2}P^2 - kQ^2 - \sqrt{\frac{-k\lambda}{6}}Q^3 + \frac{\lambda}{4!}Q^4 - \frac{3k^2}{2\lambda}. \tag{36}$$

Since the constant term $\frac{3k^2}{2\lambda}$ does not affect the dynamics of the system, we can get rid of it. However, note that by removing this term, we are removing the divergence in energy at $\lambda = 0$. Redefining the parameter $\lambda' = \sqrt{\lambda}$, this Hamiltonian can be decomposed as $H = H_0 + \lambda' H_1 + \lambda'^2 H_2$ with

$$H_0 = \frac{1}{2}P^2 - kQ^2, \tag{37}$$

$$H_1 = -\sqrt{\frac{-k}{6}}\,Q^3, \tag{38}$$

$$H_2 = \frac{Q^4}{4!}. \tag{39}$$

Analogously to the previous case, we assume that $\lambda' \ll 1$. In this setting, H_0 is just a harmonic oscillator since $k < 0$ and then plays the role of the Hamiltonian of the unperturbed problem with action-angle variables $\{I_0, \phi_0\}$ given by

$$Q(\phi_0, I_0; x) = \left(\frac{2I_0}{\omega_0}\right)^{1/2} \sin\phi_0, \tag{40a}$$

$$P(\phi_0, I_0; x) = (2\omega_0 I_0)^{1/2} \cos\phi_0. \tag{40b}$$

Here, $\omega_0 = \sqrt{-2k}$ is the frequency of the unperturbed system. In addition, the terms H_1 and H_2 are regarded as first-order and second-order potentials, respectively.

Following the same procedure as in the previous case, we first need to obtain the generating function W. The functions W_1, W_2, ... involved in (30) are again obtained from (31), but with functions Φ_μ modified by the presence of H_2. In particular, the first three functions Φ_μ are $\Phi_1 = H_1$, $\Phi_2 = H_2 + \frac{\partial W_1}{\partial \phi_0}\frac{\partial H_1}{\partial I}$ and $\Phi_3 = \frac{\partial W_1}{\partial \phi_0}\frac{\partial H_2}{\partial I} + \frac{1}{2}\left(\frac{\partial W_1}{\partial \phi_0}\right)^2 \frac{\partial^2 H_1}{\partial I^2} + \frac{\partial W_2}{\partial \phi_0}\frac{\partial H_1}{\partial I}$. The resulting functions W_μ for $\mu = 1, \ldots, 10$ are given in (A.6). Substituting these functions into (32) we get I_0, which together with (29*a*) allows us to obtain the classical deformation functions $\mathcal{O}_1 = \mathcal{O}_1(\phi_0, I; x)$ and $\mathcal{O}_2 = \mathcal{O}_2(\phi_0, I; x)$ through (26*a*) and (26*b*), respectively. In (A.7) and (A.8) we give $\mathcal{O}_1$ and $\mathcal{O}_2$ up to the first order in λ. Then, plugging $\mathcal{O}_1$ and $\mathcal{O}_2$ into (33) we arrive at the corresponding Fourier coefficients $\beta_i^{(n')}(I; x)$, explicitly shown in (A.9) and (A.10)for $n' = 0, 1, \ldots, 10$. The functions $\beta_i^{(n')}(I; x)$ for negative n' can be obtained from (A.9) and (A.10) by recalling that $\beta_i^{(-n')} = (\beta_i^{(n')})^*$.

Substituting (A.9) and (A.10) into (12), the components of the classical metric tensor for $k < 0$ are

$$g_{11}^{\rm cl} = \frac{I}{(-k)^{1/2}\lambda}\sum_{\alpha=0}^{6} c_\alpha^{(11)}\left(\frac{I\lambda}{(-k)^{3/2}}\right)^\alpha, \tag{41a}$$

$$g_{12}^{\rm cl} = \frac{(-k)^{1/2} I}{\lambda^2}\sum_{\alpha=0}^{7} c_\alpha^{(12)}\left(\frac{I\lambda}{(-k)^{3/2}}\right)^\alpha, \tag{41b}$$

$$g_{22}^{\rm cl} = \frac{(-k)^{3/2} I}{\lambda^3}\sum_{\alpha=0}^{8} c_\alpha^{(22)}\left(\frac{I\lambda}{(-k)^{3/2}}\right)^\alpha, \tag{41c}$$

where the coefficients $c_\alpha^{(11)}$, $c_\alpha^{(12)}$, and $c_\alpha^{(22)}$ are given in table 3.

4. Quantum and classical metric tensors of the quartic oscillator and the double well potential

The goal of this section is to compare the numerical QMT and analytical CMT for both cases $k > 0$ and $k < 0$. Furthermore, we compute and analyze the corresponding scalar curvatures for these metrics, which allows us to gain a better understanding of the geometry of the parameter space from both classical and quantum perspectives. With this in mind, we first need to identify the value of the action variable I and its different powers. This is done in appendix B, where we provide the corresponding identifications, which will be used for both cases $k > 0$ and $k < 0$.

We begin by computing the scalar curvature of each metric. Using (5), the scalar curvature of the analytic QMT (24) is

$$R = \sum_{\alpha=0}^{8}(-1)^{\alpha+1} d_\alpha \left(\frac{\hbar\lambda}{k^{3/2}}\right)^\alpha, \tag{42}$$

where the coefficients d_α are given in table 4. Analogously, the scalar curvatures of the CMT (34) for $k > 0$ and the CMT (41) for $k < 0$ with the identifications $I^\alpha = (f_\alpha \hbar)^\alpha$ are

Table 3. Coefficients of the classical metric tensor (41), up to order λ^5.

α	$c_\alpha^{(11)}[\times 10^{-2}]$	$c_\alpha^{(12)}[\times 10^{-2}]$	$c_\alpha^{(22)}[\times 10^{-2}]$
0	212.13	212.13	212.13
1	40.625	18.75	0
2	17.678	9.8823	4.4399
3	9.4394	5.481	2.7389
4	5.5548	3.2736	1.7019
5	3.4622	2.0555	1.0902
6	1.8352	1.0193	0.489 49
7		0.500 29	0.189 24
8			0.128 32

Table 4. Coefficients of the scalar curvatures.

α	d_α	h_α	l_α
0	28	21.1866	-4
1	30.5556	0.833 929	0
2	54.6499	60.5879	1.023 88
3	106.587	95.9538	1.849 57
4	220.2	205.334	
5	476.399	444.255	
6	1073.07	1003.07	
7	2507.83	2348.16	
8	6067.94	1574.36	

$$R^{\rm cl} = \begin{cases} \sum_{\alpha=0}^{8} (-1)^{\alpha+1} h_n \left(\frac{\hbar\lambda}{k^{3/2}}\right)^\alpha & \text{if } k > 0 \\ \sum_{\alpha=0}^{3} l_\alpha \left(\frac{\hbar\lambda}{(-k)^{3/2}}\right)^\alpha & \text{if } k < 0, \end{cases} \tag{43}$$

where the coefficients h_α and l_α are provided in table 4. From now on, we set $\hbar = 1$ to perform the comparisons between classical and quantum objects.

In figure 5 we plot the numerical QMT and the analytical CMT, as well as their corresponding scalar curvatures. Remarkable, these plots show that the CMT components for the regions $k > 0$ and $k < 0$ far from $k = 0$ agree well with the numerical QMT components, as can be seen in figures 5(a)–(c). In addition, this very good agreement is also exhibited between the determinants and scalar curvatures of the CMT and the QMT, as can be seen in figures 5(d)–(e). This proves that indeed for the regions $k > 0$ and $k < 0$ far from $k = 0$, the CMT is capable of providing the same (or almost the same) geometry of the parameter space as its quantum counterpart. However, we can also observe in figure 5 that in the vicinity of the region where $k = 0$, the components of the CMT exhibit a divergent behavior, in contrast to their quantum counterpart, which instead display a peak. The origin of this can be traced back to figure 2, where at $k = 0$, the ground state probability distribution $|\Psi_0(q)|^2$ undergoes an abrupt transition from having two maxima to having only one when moving in the $-k \rightarrow k$ direction. In the classical and perturbative quantum context this abrupt change corresponds to an exact quantum transition, which can be associated to the divergent behavior of the CMT. However, in the exact quantum sense this transition is moderated by tunneling, resulting in a precursor of a QPT associated to the maximum of the exact QMT near $k = 0$. Nonetheless, this transition can be confirmed only in the thermodynamic limit.

In figure 6, we show the numeric QMT, the analytical QMT, and the analytical CMT for $\lambda = 0.2$. Clearly, we see that indeed these metrics exhibit the same behavior for values of k far from $k = 0$. However, it is also clear that the analytic CMT and QMT diverge at $k = 0$, while the numeric QMT remains finite. This behavior is also reflected in the determinants of the corresponding metrics.

In figure 7, we show the corresponding scalar curvatures for $\lambda = 0.2$. We observe that the scalar curvatures of the numeric QMT and the CMT are in complete agreement in region $k < 0$ far form $k = 0$, where they both have the value of -4. Also, in the limit $k \rightarrow \infty$ the scalar curvature of the QMT tends to -28, while the scalar curvature of CMT tends to -21.1866, as it can be verified from (42) and (43). Thus, for the regions $k < 0$ and $k > 0$ far form $k = 0$, we have negative constant scalar curvatures, implying that the associated parameter space has a hyperbolic geometry. This is a consequence of the fact that for $k << 0$, the ground state wave function

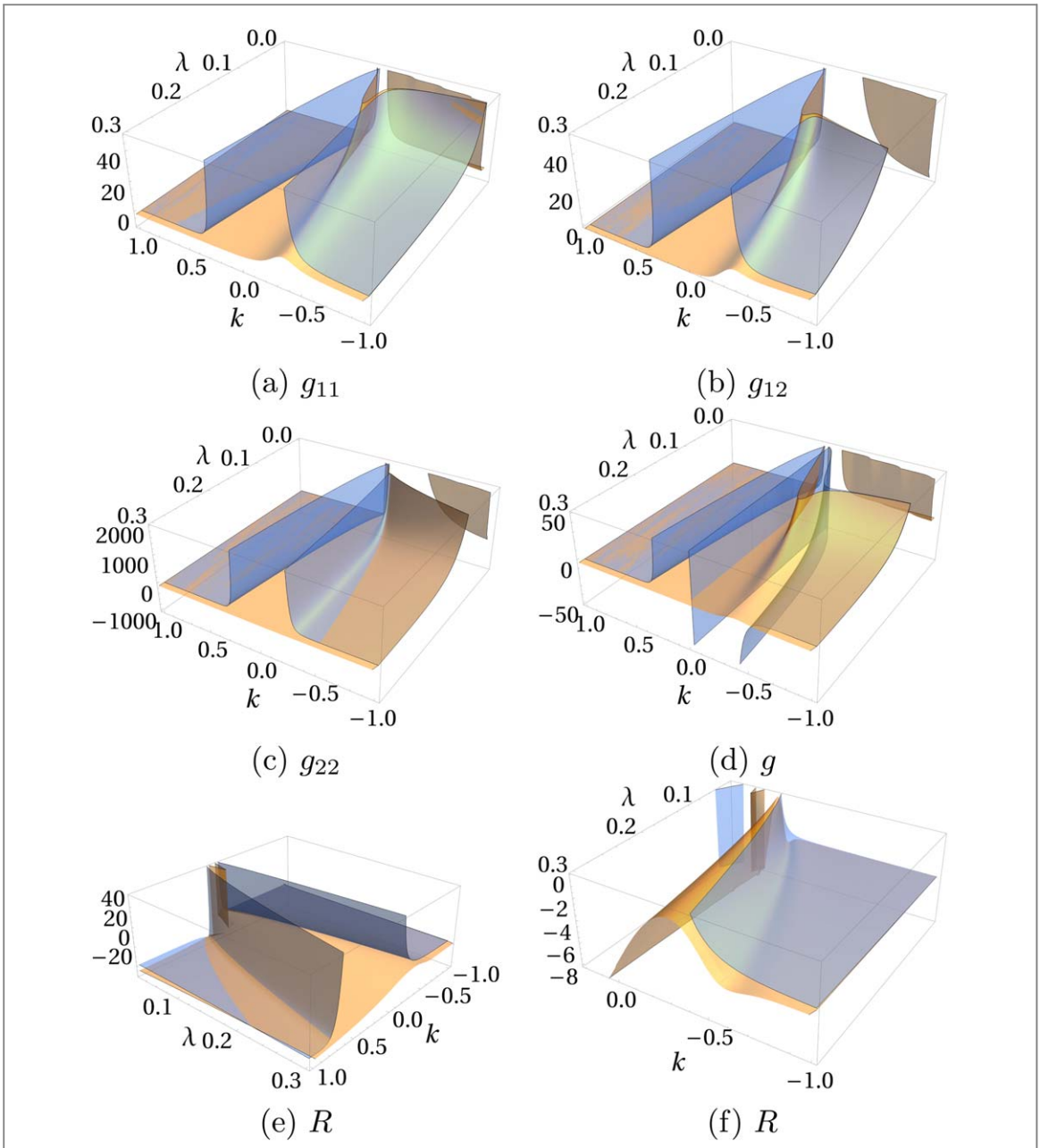

Figure 5. Comparison of parameter space metric and R obtained from the exact numerical quantum approach (orange) and the classical approach (blue). The agreement is very good except near the region where $k = 0$.

corresponds approximately to two well-located Gaussians on each of the wells, and for $k >> 0$, the ground state wave function has a dominant Gaussian term, apart from other terms that also contribute. In addition, we can see that the scalar curvature of the numeric QMT has a peak at $k = -0.245$ and a local minimum at $k = -0.48$, which are associated to the appearance of the delocalization of the probability distribution, i.e., the point where the probability density is spread out over the two wells (see figure 2). This shows that QMT can be used to predict the appearance of the delocalization of the probability distribution. Finally, notice that the scalar curvature of the CMT presents a divergent behavior at $k = 0$ that signals the appearance of the aforementioned extreme values (maximum or minimum). In this regard, it is worth noting that the scalar curvature of the analytic QMT also exhibits divergent behavior for values close to $k = 0$ (with $k > 0$).

The plots of the QMT and analytic CMT for $k = -0.5$, presented in figure 8, show an excellent agreement between the components of these metrics. This confirms the usefulness of the classical framework as a tool to be adopted in order to have a first glance over the information contained in the parameter space of a quantum system. The corresponding scalar curvatures of the numeric QMT and the analytic CMT for $k = -0.5$ are shown in figure 9. It is remarkable that both scalar curvatures tend to -4 for $\lambda \to 0$, which can also be seen from (43) in case of R^{cl} with $k < 0$. This reveals that the divergence present in the CMT can be removed by performing a change of coordinates in the parameter space. It is worth mentioning that in the case $\lambda = 0$ and

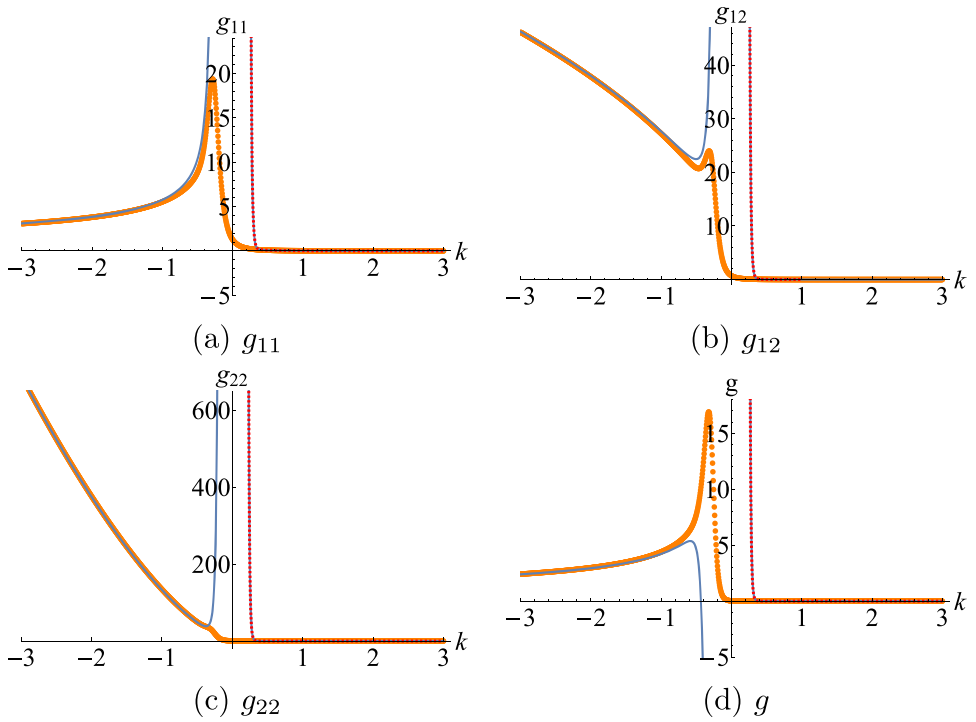

Figure 6. Comparison of the parameter space metrics for $\lambda = 0.2$. Orange round markers correspond to the exact QMT, red square markers correspond to the perturbative QTM, and the blue line corresponds to the perturbative CTM.

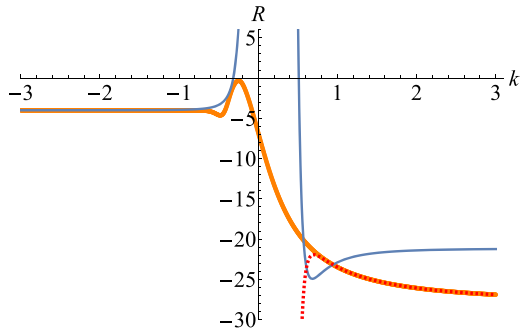

Figure 7. Comparison of the scalar curvatures for $\lambda = 0.2$. Orange round markers correspond to the exact quantum R, red square markers correspond the perturbative quantum R, and the blue line corresponds to the perturbative classical R.

$k < 0$, the Hamiltonian (25) reduces to that of an inverted harmonic oscillator, and then the classical and quantum methods used in this work cannot be applied, at least in the conventional form. On the other hand, the origin of the local minimum in the scalar curvature of the numeric QMT at $\lambda = 0.215$ may be analogous to the one of figure 7, i.e., its appearance corresponds to the separation of the probability distribution into two branches.

5. Comparison between quantum and classical approaches for the parameter space metric

The aim of this section is to carry out a more detailed analysis of the QMT (3) and CMT (13) and to strengthen the analogy between them. To do this, we employ the same identifications for powers of the action variable introduced in the previous section. In the appendix C we contrast the differences of energies that appears in (3) and (13). On the other hand, the comparison between the metrics (3) and (13) also suggests that the functions $\beta'^{(m')}_i$ are the classical analogs of quantum non-adiabatic coupling vectors $B^{(m)}_i$. In figure 10 we plot $B^{(m)}_i$ and $|\beta'^{(m')}_i|$ as functions of m and m', setting $k = 1$ and $\lambda = 0.2$. From this plot, we can see that both $B^{(m)}_i$ and $|\beta'^{(m')}_i|$ exhibit very similar behavior, approaching each other for small values of m and m'. Also, we can notice that the

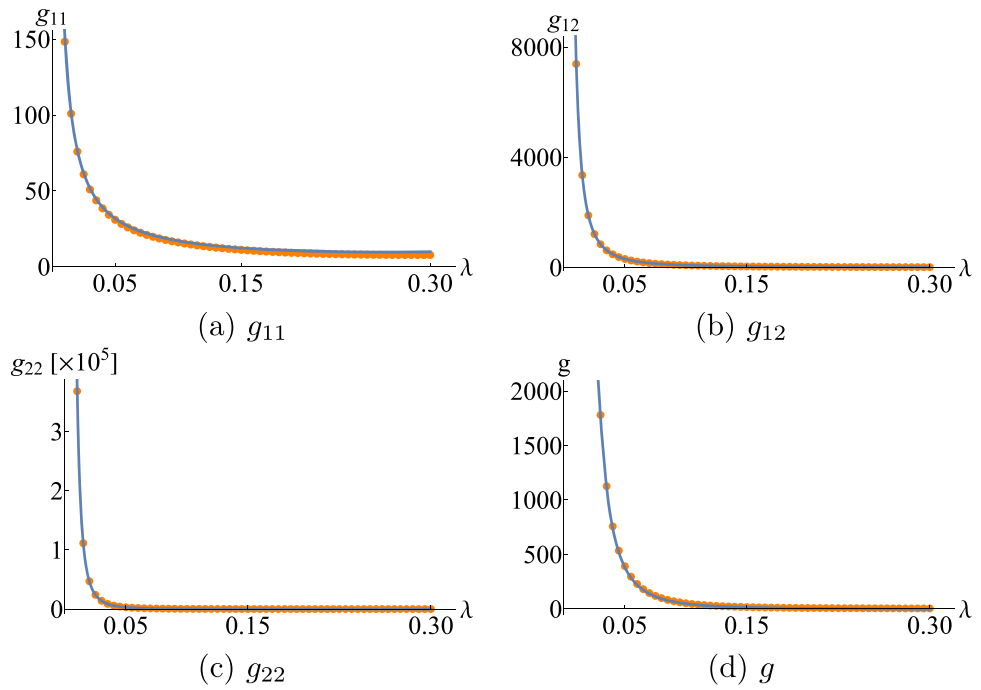

Figure 8. Comparison of the parameter space metrics for $k = -0.5$. Orange round markers correspond to the exact QMT and the blue line corresponds to the perturbative CMT.

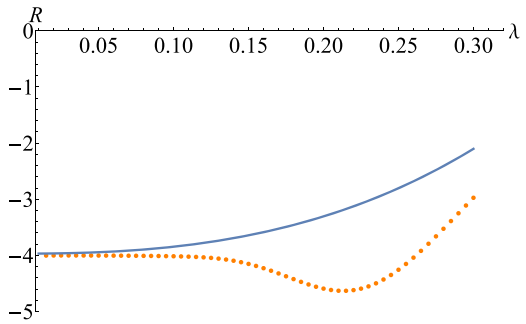

Figure 9. Comparison of the scalar curvatures for $k = -0.5$. Orange round markers correspond to the exact quantum R and the blue line corresponds to the perturbative classical R.

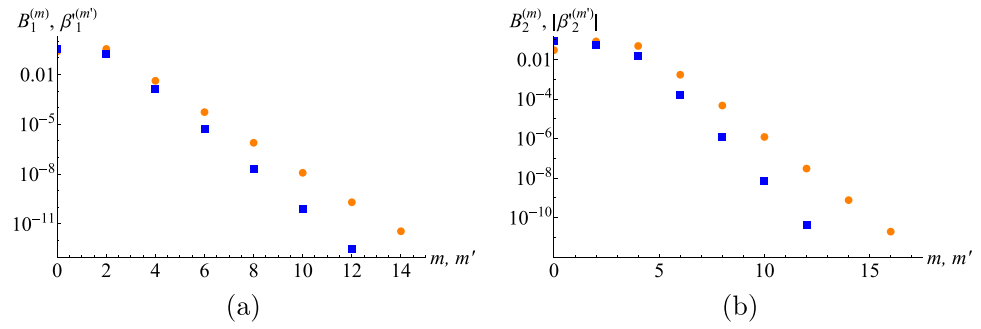

Figure 10. Comparison between $B_i^{(m)}$ and $\beta'^{(m')}_i$, with $k = 1$ and $\lambda = 0.2$. Orange round markers correspond to $B_i^{(m)}$ and blue square markers correspond to $\beta'^{(m')}_i$.

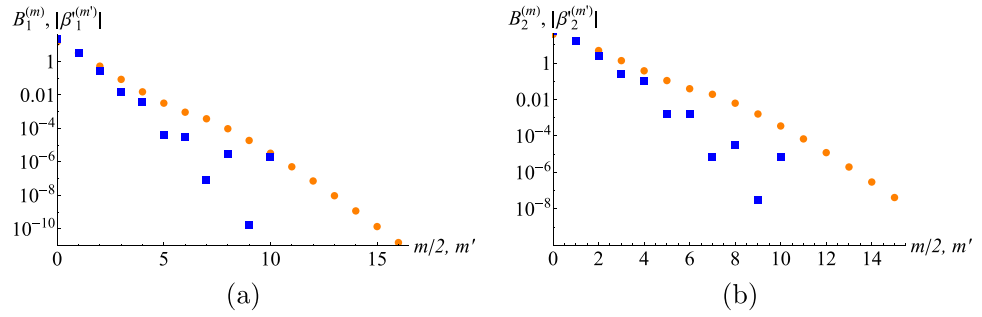

Figure 11. Comparison between $B_i^{(m)}$ and $\beta'^{(m')}_i$, with $k = -1$ and $\lambda = 0.2$. Orange round markers correspond to $B_i^{(m)}$ and blue square markers correspond to $|\beta'^{(m')}_i|$.

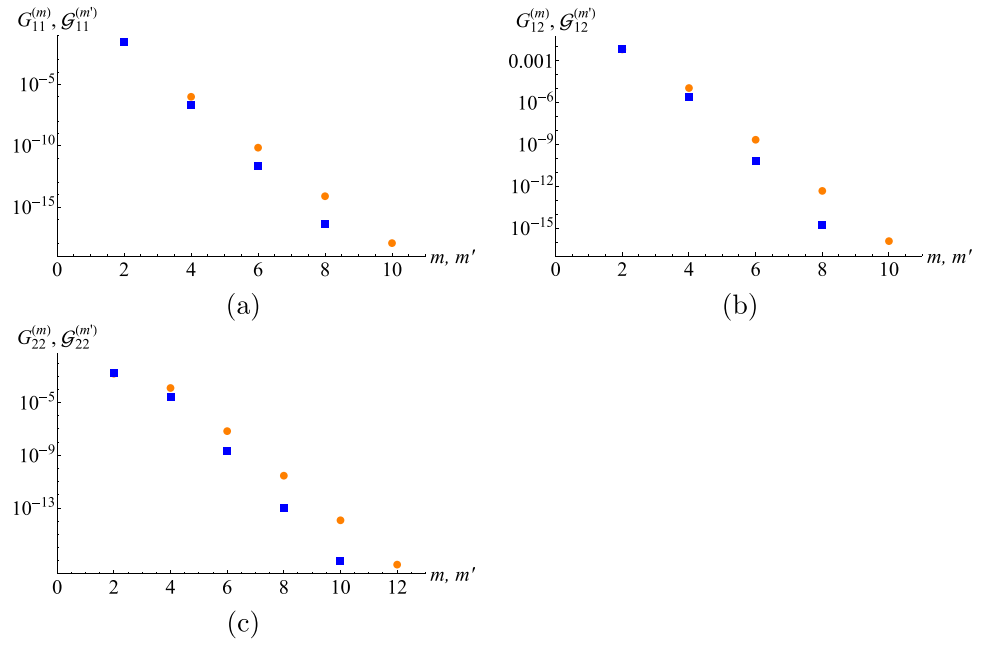

Figure 12. Comparison between $G_{ij}^{(m)}$ and $\mathcal{G}_{ij}^{(m')}$, with $k = 1$ and $\lambda = 0.2$. Orange round markers correspond to $G_{ij}^{(m)}$ and blue square markers correspond to $\mathcal{G}_{ij}^{(m')}$.

classical functions $\beta'^{(m')}_i$ tend to zero faster than their quantum counterparts $B_i^{(m)}$. Remarkably and reinforcing the analogy, for odd m and m' both functions $B_i^{(m)}$ and $\beta'^{(m')}_i$ are zero. This is the reason whyonly the values of $B_i^{(m)}$ and $\beta'^{(m')}_i$ for even m and m' appear in the plot.

In the case $k = -1$ and $\lambda = 0.2$, the functions $\beta'^{(m')}_i$ are real for even m' and purely imaginary for odd m'. However, for the same values of k and λ, the coupling vectors $B_i^{(m)}$ are real for even m and vanishes for odd m. In figure 11, we plot $B_i^{(m)}$ as function of $m/2$ and $|\beta'^{(m')}_i|$ as function of m'. This plot illustrates the analogous behavior of $B_i^{(m)}$ and $|\beta'^{(m')}_i|$, showing that our classical analog corresponds well to the coupling vectors of the quantum case. We have plotted $B_i^{(m)}$ as a function of $m/2$ because of the quasi-degeneration resulting from the double-well potential, which does not have a classical counterpart.

To aid in a better understanding of this, in figures 12 we show $G_{ij}^{(m)}$ and $\mathcal{G}_{ij}^{(m')}$ for $k = 1$ and $\lambda = 0.2$. We see that the significant contributions of $G_{ij}^{(m)}$ and $\mathcal{G}_{ij}^{(m')}$ to their metrics occur for $m \leqslant 4$ and $m' \leqslant 4$, and that precisely for these values of m and m' there is good agreement between these quantities. For $m > 4$ and $m' > 4$, the contributions of $G_{ij}^{(m)}$ and $\mathcal{G}_{ij}^{(m')}$ are of the order of 10^{-5} or smaller.

In the case $k = -1$ and $\lambda = 0.2$, the classical function $\mathcal{G}_{ij}^{(m')}$ is real for all m', since the product $\beta'^{(m')}_i(\beta'^{(m')}_j)^*$ is real because $\beta_i^{(m')}$ is real for even m' and pure imaginary for odd m'. In the quantum case, the function $G_{ij}^{(m)}$ is nonzero for even m and zero for odd m. Clearly, this is because the non-adiabatic coupling

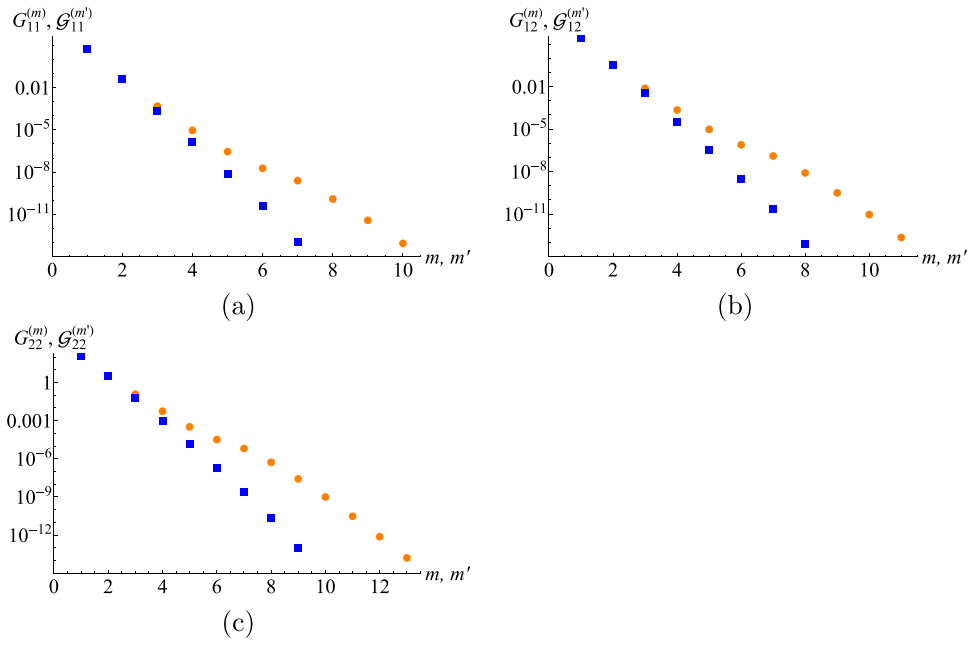

Figure 13. Comparison between $G_{ij}^{(m)}$ and $\mathcal{G}_{ij}^{(m')}$, with $k = -1$ and $\lambda = 0.2$. Orange round markers correspond to $G_{ij}^{(m)}$ and blue square markers correspond to $\mathcal{G}_{ij}^{(m')}$.

vector $B_i^{(m)}$ is nonzero for even m and zero for odd m. In figure 13 we plot $G_{ij}^{(m)}$ and $\mathcal{G}_{ij}^{(m')}$ as functions of m and m' for $k = -1$ and $\lambda = 0.2$. Here we can also appreciate that the relevant contributions of $G_{ij}^{(m)}$ and $\mathcal{G}_{ij}^{(m')}$ to the quantum and classical metrics, respectively, occur for $m \leqslant 5$ and $m' \leqslant 5$. Certainly, the contributions of $G_{ij}^{(m)}$ and $\mathcal{G}_{ij}^{(m')}$ are of the order of10^{-5} or smaller for $m > 5$ and $m' > 5$. These results suggest that our classical approach could be used to get a first idea of the parameter space geometry for the first quantum states.

6. Conclusions

In this paper, we have studied the geometry of the parameter space of the single-well anharmonic oscillator ($k > 0$) and the quartic double-well potential ($k < 0$), computing the QMT and the CMT, as well as their scalar curvatures. In the quantum setting, we used an exact numerical diagonalization, and a perturbative treatment in the parameter λ to obtain the ground-state wave function up to 10th order in λ. In the classical framework, we introduce a formulation of the CMT based on Fourier series [23] to obtain the CMT up to the 10th order in λ for the single-well system and up to 6th order in λ for the double-well system.

Identifying the different powers of the action variable that arise from the semiclassical relation (B.1) between the analytic classical and quantum metrics of the single-well problem, we found that the QMT and the CMT and their corresponding scalar curvatures have a very close behavior except in points near $k = 0$, as shown in figure 5.

For a fixed value of λ, far from $k = 0$, when $k < 0$, both classical and quantum scalar curvatures take the value of -4, indicating that the associated parameter space has a hyperbolic geometry in that region. In contrast, for $k > 0$ these scalar curvatures do not coincide, probably because in this case the ground state wave function is not fully Gaussian. The CMT and its curvature show a divergent behavior at $k = 0$, which could be associated with the peaks exhibited by the exact scalar curvature, indicating the appearance of a delocalization of the probability distribution. For a constant, negative value of k, we found a remarkable agreement between the numeric QMT and analytic CMT, both showing a divergent behavior for $\lambda \to 0$. At this limit, the scalar curvatures of both metrics tend to -4, meaning that the singularity at $\lambda \to 0$ is apparent and can be removed by performing a change of coordinates (parameters). In this case, it is also worth mentioning that the scalar curvature of the QMT has a local minimum, which is absent in its classical counterpart and could be related to a separation of the probability distribution into two branches.

We also compared in detail the perturbative expression of QMT with the Fourier-based expression of the CMT, exhibiting their close relationship, supporting the view that the CMT acts as the classical version of QMT. Furthermore, we can say that taking into account the three analysis procedures used, the calculation of the quantum metric tensor gives us an excellent description of the delocalization of the wave function in the case of

the double well potential. This is even achieved from the classical point of view, showing that the tool has a global view of the system as long as it is worked in the appropriate variables, such as angle-action variables. In this spirit, the present results can be expanded in future works to more general situations, such as showing if our classical approximation allows for an acceptable description near the maximum of potential, as it has done in the case of the double well, for example in the Lipkin-Meshkov-Glick model [43] or in the case of the inverted harmonic oscillator [44, 45]. In addition, it would be interesting to study how classical formalism might be expanded to provide an initial insight into the parameter space associated with the first excited states. Finally, given that the classical analog of the non-adiabatic coupling vectors has been obtained, it would be interesting to show if our classical description has any application in molecular modeling [46].

Acknowledgments

We acknowledge the support of the Computing Center-ICN, in particular, of E Palacios, L Díaz, and E Murrieta. This work was partially supported by DGAPA-PAPIIT Grants No. IN105422 and IN109523. D.G. acknowledges the financial support of Instituto Politécnico Nacional, Grant No. SIP-20230323, and the postdoctoral fellowship from Consejo Nacional de Humanidades, Ciencia y Tecnología (CONAHCyT), México.

Data availability statement

All data that support the findings of this study are included within the article (and any supplementary files).

Appendix A. Generating functions and Fourier coefficients

Case $k > 0$

Functions W_μ for $\mu = 1, \ldots, 10$:

$$W_1 = -\frac{I^2}{192k^{3/2}}(-8\sin(2\phi_0) + \sin(4\phi_0)), \tag{A.1a}$$

$$W_2 = \frac{I^3}{55296k^3}(-384\sin(2\phi_0) + 132\sin(4\phi_0) - 32\sin(6\phi_0) + 3\sin(8\phi_0)), \tag{A.1b}$$

$$W_3 = \frac{I^4}{5308416k^{9/2}}(9264\sin(2\phi_0) - 4101\sin(4\phi_0) + 1624\sin(6\phi_0) - 441\sin(8\phi_0) + 72\sin(10\phi_0) - 5\sin(12\phi_0)), \tag{A.1c}$$

$$W_4 = \frac{I^5}{21233664k^6}\left(-11408\sin(2\phi_0) + 5644\sin(4\phi_0) - 2768\sin(6\phi_0) + \frac{2171}{2}\sin(8\phi_0) - 320\sin(10\phi_0) + 65\sin(12\phi_0) - 8\sin(14\phi_0) + \frac{7}{16}\sin(16\phi_0)\right), \tag{A.1d}$$

$$W_5 = \frac{7I^6}{122305904640k^{15/2}}(3261840\sin(2\phi_0) - 1713090\sin(4\phi_0) + 945280\sin(6\phi_0) - 450270\sin(8\phi_0) + 176832\sin(10\phi_0) - 54575\sin(12\phi_0) + 12600\sin(14\phi_0) - 2025\sin(16\phi_0) + 200\sin(18\phi_0) - 9\sin(20\phi_0)), \tag{A.1e}$$

$$W_6 = \frac{I^7}{48922361856k^9}\left(-3438784\sin(2\phi_0) + \frac{3744541}{2}\sin(4\phi_0) - 1111556\sin(6\phi_0) + \frac{9550433}{16}\sin(8\phi_0) - 278530\sin(10\phi_0) + \frac{436033}{4}\sin(12\phi_0) - 34744\sin(14\phi_0) + \frac{69727}{8}\sin(16\phi_0) - \frac{4936}{3}\sin(18\phi_0) + \frac{873}{4}\sin(20\phi_0) - 18\sin(22\phi_0) + \frac{11}{16}\sin(24\phi_0)\right), \tag{A.1f}$$

$$W_7 = \frac{I^8}{350675489783808k^{21/2}}(9825412576\sin(2\phi_0) - 5476716371\sin(4\phi_0) + 3414796056\sin(6\phi_0) - 1987448015\sin(8\phi_0) + 1040341960\sin(10\phi_0) - 475378323\sin(12\phi_0) + 185530096\sin(14\phi_0) - 60516911\sin(16\phi_0) + 16101008\sin(18\phi_0) - 3387615\sin(20\phi_0) + 539784\sin(22\phi_0) - 60907\sin(24\phi_0) + 4312\sin(26\phi_0) - 143\sin(28\phi_0)), \tag{A.1g}$$

$$W_8 = \frac{I^9}{1803473947459584k^{12}}\left(-21017661600\sin(2\phi_0) + 11907018980\sin(4\phi_0) - \frac{23057409280}{3}\sin(6\phi_0) + 4736665695\sin(8\phi_0) - 2690310560\sin(10\phi_0) + 1370942900\sin(12\phi_0) - 615537920\sin(14\phi_0) + \frac{479168405}{2}\sin(16\phi_0) - \frac{238607680}{3}\sin(18\phi_0) + 22109724\sin(20\phi_0) - 5031712\sin(22\phi_0) + \frac{2729749}{3}\sin(24\phi_0) - 125312\sin(26\phi_0) + 12298\sin(28\phi_0) - \frac{2288}{3}\sin(30\phi_0) + \frac{715}{32}\sin(32\phi_0)\right), \tag{A.1h}$$

$$W_9 = \frac{11I^{10}}{623280596242032230 4k^{27/2}}(2838604924368\sin(2\phi_0) - 1627087268250\sin(4\phi_0) + 1077391402752\sin(6\phi_0)$$
$$-692748547848\sin(8\phi_0) + 418042653696\sin(10\phi_0) - 230923291308\sin(12\phi_0) + 114908848992\sin(14\phi_0)$$
$$-50823988380\sin(16\phi_0) + 19735646368\sin(18\phi_0) - 6642798660\sin(20\phi_0) + 1910480256\sin(22\phi_0)$$
$$-461485548\sin(24\phi_0) + 91604736\sin(26\phi_0) - 14510691\sin(28\phi_0)$$
$$+1758744\sin(30\phi_0) - 152685\sin(32\phi_0) + 8424\sin(34\phi_0) - 221\sin(36\phi_0)), \tag{A.1i}$$

$$W_{10} = \frac{I^{11}}{4155203974946881536k^{15}}(-9186469977056\sin(2\phi_0) + 5311969531237\sin(4\phi_0) - 3586272994472\sin(6\phi_0)$$
$$+\frac{9528014994589}{4}\sin(8\phi_0) - \frac{7529224160272}{5}\sin(10\phi_0) + 884878319954\sin(12\phi_0) - 476281378048\sin(14\phi_0)$$
$$+\frac{464168079361}{2}\sin(16\phi_0) - 101347955904\sin(18\phi_0) + \frac{196368227671}{5}\sin(20\phi_0) - 13367025784\sin(22\phi_0)$$
$$+\frac{63203940789}{16}\sin(24\phi_0) - 999988518\sin(26\phi_0) + \frac{853040643}{4}\sin(28\phi_0) - \frac{187506696}{5}\sin(30\phi_0)$$
$$+\frac{42255655}{8}\sin(32\phi_0) - 571480\sin(34\phi_0) + \frac{177905}{4}\sin(36\phi_0) - 2210\sin(38\phi_0) + \frac{4199}{80}\sin(40\phi_0)\Big). \tag{A.1j}$$

Classical functions $\mathcal{O}_1(\phi_0, I; x)$ and $\mathcal{O}_2(\phi_0, I; x)$ up to the fourth order in λ (the complete list can be obtained under request):

$$\mathcal{O}_1 = \frac{I}{k^{1/2}}\sin^2(\phi_0) - \frac{I^2\lambda}{192k^2}(-16\cos(2\phi_0) + 4\cos(4\phi_0))\sin^2(\phi_0) + \frac{I^3\lambda^2}{55296k^{7/2}}(-768\cos(2\phi_0)$$
$$+528\cos(4\phi_0) - 192\cos(6\phi_0) + 24\cos(8\phi_0))\sin^2(\phi_0) + \frac{I^4\lambda^3}{5308416k^5}(18528\cos(2\phi_0)$$
$$-16404\cos(4\phi_0) + 9744\cos(6\phi_0) - 3528\cos(8\phi_0) + 720\cos(10\phi_0) - 60\cos(12\phi_0))\sin^2(\phi_0)$$
$$+\frac{I^5\lambda^4}{21233664k^{13/2}}(-22816\cos(2\phi_0) + 22576\cos(4\phi_0) - 16608\cos(6\phi_0) + 8684\cos(8\phi_0)$$
$$-3200\cos(10\phi_0) + 780\cos(12\phi_0) - 112\cos(14\phi_0) + 7\cos(16\phi_0))\sin^2(\phi_0), \tag{A.2}$$

$$\mathcal{O}_2 = \frac{I^2}{6k}\sin^4(\phi_0) - \frac{I^3\lambda}{576k^{5/2}}(-16\cos(2\phi_0) + 4\cos(4\phi_0))\sin^4(\phi_0) + \frac{I^4\lambda^2}{13824k^4}(-64\cos(2\phi_0)$$
$$+16\cos^2(2\phi_0) + 44\cos(4\phi_0)$$
$$-8\cos(2\phi_0)\cos(4\phi_0) + \cos^2(4\phi_0) - 16\cos(6\phi_0) + 2\cos(8\phi_0))\sin^4(\phi_0)$$
$$+\frac{I^5\lambda^3}{k^{11/2}}\Big(-\frac{1}{31850496}(-16\cos(2\phi_0) + 4\cos(4\phi_0))(-768\cos(2\phi_0) + 528\cos(4\phi_0) - 192\cos(6\phi_0) + 24\cos(8\phi_0))\sin^4(\phi_0)$$
$$+\frac{1}{c}(18528\cos(2\phi_0) - 16404\cos(4\phi_0) + 9744\cos(6\phi_0) - 3528\cos(8\phi_0) + 720\cos(10\phi_0)$$
$$-60\cos(12\phi_0))\sin^4(\phi_0)) + \frac{I^6\lambda^4}{k^7}\Big(\frac{1}{18345885696}(-768\cos(2\phi_0) + 528\cos(4\phi_0) - 192\cos(6\phi_0)$$
$$+24\cos(8\phi_0))^2\sin^4(\phi_0) - \frac{1}{3057647616}(-16\cos(2\phi_0) + 4\cos(4\phi_0))(18528\cos(2\phi_0)$$
$$-16404\cos(4\phi_0) + 9744\cos(6\phi_0) - 3528\cos(8\phi_0)$$
$$+720\cos(10\phi_0) - 60\cos(12\phi_0))\sin^4(\phi_0) + \frac{1}{63700992}(-22816\cos(2\phi_0) + 22576\cos(4\phi_0)$$
$$-16608\cos(6\phi_0) + 8684\cos(8\phi_0) - 3200\cos(10\phi_0) + 780\cos(12\phi_0) - 112\cos(14\phi_0)$$
$$+7\cos(16\phi_0))\sin^4(\phi_0)). \tag{A.3}$$

Coefficients $\beta_1^{(n')}(I; x)$ and $\beta_2^{(n')}(I; x)$ for $n' = 0, \pm1, \ldots, \pm10$:

$$\beta_1^{(0)} = \frac{I}{2\sqrt{k}} - \frac{I^2\lambda}{16k^2} + \frac{85I^3\lambda^2}{4608k^{7/2}} - \frac{125I^4\lambda^3}{18432k^5} + \frac{39193I^5\lambda^4}{14155776k^{13/2}} - \frac{204281I^6\lambda^5}{169869312k^8} + \frac{17750261I^7\lambda^6}{32614907904k^{19/2}}$$
$$-\frac{132347765I^8\lambda^7}{521838526464k^{11}} + \frac{435757124275I^9\lambda^8}{3606947894919168k^{25/2}} - \frac{281528168779I^{10}\lambda^9}{4809263859892224k^{14}} + \frac{79655597681647I^{11}\lambda^{10}}{2770135983297921024k^{31/2}}, \tag{A.4a}$$

$$\beta_1^{(\pm2)} = -\frac{I}{4\sqrt{k}} + \frac{5I^2\lambda}{192k^2} - \frac{83I^3\lambda^2}{12288k^{7/2}} + \frac{3965I^4\lambda^3}{1769472k^5} - \frac{94969I^5\lambda^4}{113246208k^{13/2}} + \frac{5502505I^6\lambda^5}{16307453952k^8} - \frac{446236787I^7\lambda^6}{3131031158784k^{19/2}}$$
$$+\frac{1040920667I^8\lambda^7}{16698832846848k^{11}} - \frac{4038351097037I^9\lambda^8}{14427791579676672k^{25/2}} + \frac{2221131730877I^{10}\lambda^9}{17313349895612006 4k^{14}} - \frac{198708866965765I^{11}\lambda^{10}}{3324163179957505228 8k^{31/2}}, \tag{A.4b}$$

$$\beta_1^{(\pm4)} = \frac{I^2\lambda}{192k^2} - \frac{11I^3\lambda^2}{4608k^{7/2}} + \frac{479I^4\lambda^3}{442368k^5} - \frac{3557I^5\lambda^4}{7077888k^{13/2}} + \frac{3888053I^6\lambda^5}{16307453952k^8} - \frac{15026351I^7\lambda^6}{130459631616k^{19/2}}$$
$$+\frac{2121579677I^8\lambda^7}{37572373905408k^{11}} - \frac{505281382871^9\lambda^8}{1803473947459584k^{25/2}} + \frac{19446977965327I^{10}\lambda^9}{1385067991648960512k^{14}} - \frac{235859488654553I^{11}\lambda^{10}}{3324163179957505228 8k^{31/2}}, \tag{A.4c}$$

$$\beta_1^{(\pm 6)} = -\frac{I^3\lambda^2}{12288k^{7/2}} + \frac{13I^4\lambda^3}{196608k^5} - \frac{395I^5\lambda^4}{9437184k^{13/2}} + \frac{66187I^6\lambda^5}{2717908992k^8} - \frac{791329I^7\lambda^6}{57982058496k^{19/2}} + \frac{62666879I^8\lambda^7}{8349416423424k^{11}} - \frac{4366456033I^9\lambda^8}{1068725302198272k^{25/2}} + \frac{1134423343811I^{10}\lambda^9}{51298814505517056k^{14}} - \frac{11751695020477I^{11}\lambda^{10}}{9849372385059274752k^{31/2}}, \tag{A.4d}$$

$$\beta_1^{(\pm 8)} = \frac{I^4\lambda^3}{884736k^5} - \frac{7I^5\lambda^4}{5308416k^{13/2}} + \frac{545I^6\lambda^5}{509607936k^8} - \frac{36581I^7\lambda^6}{48922361856k^{19/2}} + \frac{28045I^8\lambda^7}{57982058496k^{11}} - \frac{8418031I^9\lambda^8}{28179280429056k^{25/2}} + \frac{3875661979I^{10}\lambda^9}{21641687369515008k^{14}} - \frac{218564097493I^{11}\lambda^{10}}{2077601987473440768k^{31/2}}, \tag{A.4e}$$

$$\beta_1^{(\pm 10)} = -\frac{5I^5\lambda^4}{339738624k^{13/2}} + \frac{365I^6\lambda^5}{16307453952k^8} - \frac{2165I^7\lambda^6}{97844723712k^{19/2}} + \frac{1357895I^8\lambda^7}{75144747810816k^{11}} - \frac{63775105I^9\lambda^8}{4809263859892224k^{25/2}} + \frac{6300898345I^{10}\lambda^9}{692533995824480256k^{14}} - \frac{99135644645I^{11}\lambda^{10}}{16620815899787526144k^{31/2}}, \tag{A.4f}$$

$$\beta_1^{(\pm 12)} = \frac{I^6\lambda^5}{5435817984k^8} - \frac{5I^7\lambda^6}{14495514624k^{19/2}} + \frac{1679I^8\lambda^7}{4174708211712k^{11}} - \frac{225889I^9\lambda^8}{601157982486528k^{25/2}} + \frac{11872213I^{10}\lambda^9}{38474110879137792k^{14}} - \frac{107583905I^{11}\lambda^{10}}{461689330549653504k^{31/2}}, \tag{A.4g}$$

$$\beta_1^{(\pm 14)} = -\frac{7I^7\lambda^6}{3131031158784k^{19/2}} + \frac{749I^8\lambda^7}{150289495621632k^{11}} - \frac{48293I^9\lambda^8}{7213895789838336k^{25/2}} + \frac{1625743I^{10}\lambda^9}{23084466527482675 2k^{14}} - \frac{851071067I^{11}\lambda^{10}}{132966527198300209152k^{31/2}}. \tag{A.4h}$$

$$\beta_2^{(0)} = \frac{I^2}{16k} - \frac{17I^3\lambda}{1152k^{5/2}} + \frac{125I^4\lambda^2}{24576k^4} - \frac{3563I^5\lambda^3}{1769472k^{11/2}} + \frac{145915I^6\lambda^4}{169869312k^7} - \frac{1044133I^7\lambda^5}{2717908992k^{17/2}} + \frac{185286871I^8\lambda^6}{1043677052928k^{10}} - \frac{18945961925I^9\lambda^7}{225434243432448k^{23/2}} + \frac{21656012983I^{10}\lambda^8}{534362651099136k^{13}} - \frac{137337237382151^{11}\lambda^9}{692533995824480256k^{29/2}} + \frac{408045475787951^{12}\lambda^{10}}{4155203974946881536k^{16}}, \tag{A.5a}$$

$$\beta_2^{(\pm 2)} = -\frac{I^2}{24k} + \frac{7I^3\lambda}{768k^{5/2}} - \frac{655I^4\lambda^2}{221184k^4} + \frac{11855I^5\lambda^3}{10616832k^{11/2}} - \frac{310421I^6\lambda^4}{679477248k^7} + \frac{9634829I^7\lambda^5}{48922361856k^{17/2}} - \frac{1654242575I^8\lambda^6}{18786186952704k^{10}} + \frac{729534105711^9\lambda^7}{1803473947459584k^{23/2}} - \frac{2737674498471^{10}\lambda^8}{1442779157967 6672k^{13}} + \frac{250698423235931^{11}\lambda^9}{2770135983297921024k^{29/2}} - \frac{872657478596255I^{12}\lambda^{10}}{19944979079745031372 8k^{16}}, \tag{A.5b}$$

$$\beta_2^{(\pm 4)} = \frac{I^2}{96k} - \frac{I^3\lambda}{768k^{5/2}} + \frac{13I^4\lambda^2}{73728k^4} + \frac{113I^5\lambda^3}{10616832k^{11/2}} - \frac{257515I^6\lambda^4}{8153726976k^7} + \frac{4700251I^7\lambda^5}{195689447424k^{17/2}} - \frac{10397377I^8\lambda^6}{695784701952k^{10}} + \frac{7786939537I^9\lambda^7}{901736973729792k^{23/2}} - \frac{3338632139569I^{10}\lambda^8}{692533995824480256k^{13}} + \frac{43927833582367I^{11}\lambda^9}{16620815899787526144k^{29/2}} - \frac{2288575869972055I^{12}\lambda^{10}}{15955983263796025098 24k^{16}}, \tag{A.5c}$$

$$\beta_2^{(\pm 6)} = -\frac{I^3\lambda}{2304k^{5/2}} + \frac{17I^4\lambda^2}{73728k^4} - \frac{779I^5\lambda^3}{7077888k^{11/2}} + \frac{52805I^6\lambda^4}{1019215872k^7} - \frac{532487I^7\lambda^5}{21743271936k^{17/2}} + \frac{18274109I^8\lambda^6}{1565515579392k^{10}} - \frac{1124861431I^9\lambda^7}{200385994162176k^{23/2}} + \frac{52366851143I^{10}\lambda^8}{19237055439568896k^{13}} - \frac{2456402477509I^{11}\lambda^9}{18467573221986140 16k^{29/2}} + \frac{10440303294024551^{12}\lambda^{10}}{15955983263796025098 24k^{16}}, \tag{A.5d}$$

$$\beta_2^{(\pm 8)} = \frac{5I^4\lambda^2}{442368k^4} - \frac{I^5\lambda^3}{98304k^{11/2}} + \frac{1741I^6\lambda^4}{254803968k^7} - \frac{100921I^7\lambda^5}{24461180928k^{17/2}} + \frac{1854211I^8\lambda^6}{782757789696k^{10}} - \frac{18650465I^9\lambda^7}{14089640214528k^{23/2}} + \frac{291825893I^{10}\lambda^8}{400771988324352k^{13}} - \frac{412152359593I^{11}\lambda^9}{1038800993736720384k^{29/2}} + \frac{76200897469177I^{12}\lambda^{10}}{3545774058621338910 72k^{16}}, \tag{A.5e}$$

$$\beta_2^{(\pm 10)} = -\frac{5I^5\lambda^3}{21233664k^{11/2}} + \frac{605I^6\lambda^4}{2038431744k^7} - \frac{49655I^7\lambda^5}{195689447424k^{17/2}} + \frac{1730915I^8\lambda^6}{9393093476352k^{10}} - \frac{221147005I^9\lambda^7}{1803473947459584k^{23/2}} + \frac{1116576365I^{10}\lambda^8}{1442779157967 6672k^{13}} - \frac{1307027180951^{11}\lambda^9}{2770135983297921024k^{29/2}} + \frac{2074888959351^{12}\lambda^{10}}{7387029288794456064k^{16}}, \tag{A.5f}$$

$$\beta_2^{(\pm 12)} = \frac{35I^6\lambda^4}{8153726976k^7} - \frac{151I^7\lambda^5}{21743271936k^{17/2}} + \frac{45013I^8\lambda^6}{6262062317568k^{10}} - \frac{5484323I^9\lambda^7}{901736973729792k^{23/2}} + \frac{264896183I^{10}\lambda^8}{57711166318706688k^{13}} - \frac{2230866583I^{11}\lambda^9}{692533995824480256k^{29/2}} + \frac{429090687803I^{12}\lambda^{10}}{19944979079745031372 8k^{16}}, \tag{A.5g}$$

$$\beta_2^{(\pm 14)} = -\frac{7I^7\lambda^5}{97844723712k^{17/2}} + \frac{2653I^8\lambda^6}{18786186952704k^{10}} - \frac{309169I^9\lambda^7}{1803473947459584k^{23/2}} + \frac{1591303I^{10}\lambda^8}{9618527719784448k^{13}} - \frac{2319042901I^{11}\lambda^9}{16620815899787526144k^{29/2}} + \frac{3581080741I^{12}\lambda^{10}}{33241631799575052288k^{16}}. \tag{A.5h}$$

Case $k < 0$

Functions W_μ for $\mu = 1, \ldots, 10$:

$$W_1 = \frac{I^{3/2}}{12\sqrt[4]{2}\sqrt{3}(-k)^{3/4}}(-9\cos(\phi_0) + \cos(3\phi_0)), \tag{A.6a}$$

$$W_2 = -\frac{I^2}{384\sqrt{2}(-k)^{3/2}}(37\sin(2\phi_0) - 8\sin(4\phi_0) + \sin(6\phi_0)), \tag{A.6b}$$

$$W_3 = -\frac{I^{5/2}}{18432\ 2^{3/4}\sqrt{3}(-k)^{9/4}}(2406\cos(\phi_0) - 888\cos(3\phi_0) + 336\cos(5\phi_0) - 69\cos(7\phi_0) + 7\cos(9\phi_0)), \tag{A.6c}$$

$$W_4 = -\frac{I^3}{442368k^3}(-6504\sin(2\phi_0) + 2841\sin(4\phi_0) - 1188\sin(6\phi_0) + 348\sin(8\phi_0) - 60\sin(10\phi_0) + 5\sin(12\phi_0)), \tag{A.6d}$$

$$W_5 = \frac{I^{7/2}}{188743680\sqrt[4]{2}\sqrt{3}(-k)^{15/4}}(-4906185\cos(\phi_0) + 2061605\cos(3\phi_0) - 1134741\cos(5\phi_0) + 505545\cos(7\phi_0) - 175085\cos(9\phi_0) + 41865\cos(11\phi_0) - 6105\cos(13\phi_0) + 429\cos(15\phi_0)), \tag{A.6e}$$

$$W_6 = -\frac{I^4}{84934656\sqrt{2}(-k)^{9/2}}(601389\sin(2\phi_0) - 305226\sin(4\phi_0) + 170369\sin(6\phi_0) - 81906\sin(8\phi_0) + 31413\sin(10\phi_0) - 9106\sin(12\phi_0) + 1839\sin(14\phi_0) - 231\sin(16\phi_0) + 14\sin(18\phi_0)), \tag{A.6f}$$

$$W_7 = -\frac{I^{9/2}}{1217623228416\ 2^{3/4}\sqrt{3}(-k)^{21/4}}(17403059940\cos(\phi_0) - 7561686566\cos(3\phi_0) + 4693975146\cos(5\phi_0) - 2657276376\cos(7\phi_0) + 1330840168\cos(9\phi_0) - 552365079\cos(11\phi_0) + 181745025\cos(13\phi_0) - 45127082\cos(15\phi_0) + 7885878\cos(17\phi_0) - 867867\cos(19\phi_0) + 46189\cos(21\phi_0)), \tag{A.6g}$$

$$W_8 = \frac{I^5}{217432719360k^6}(-46426448\sin(2\phi_0) + 24902680\sin(4\phi_0) - 15580848\sin(6\phi_0) + 9103525\sin(8\phi_0) - 4689512\sin(10\phi_0) + 2060452\sin(12\phi_0) - 744152\sin(14\phi_0) + 213052\sin(16\phi_0) - 46216\sin(18\phi_0) + 7116\sin(20\phi_0) - 696\sin(22\phi_0) + 33\sin(24\phi_0)), \tag{A.6h}$$

$$W_9 = \frac{I^{11/2}}{64123518131896324\sqrt{2}\sqrt{3}(-k)^{27/4}}(-29825420608692\cos(\phi_0) + 13119866088564\cos(3\phi_0) - 8590881168369\cos(5\phi_0) + 5419669290273\cos(7\phi_0) - 3209105952051\cos(9\phi_0) + 1696298165091\cos(11\phi_0) - 777910346658\cos(13\phi_0) + 301429404354\cos(15\phi_0) - 95900963886\cos(17\phi_0) + 24247831374\cos(19\phi_0) - 4668334827\cos(21\phi_0) + 642333627\cos(23\phi_0) - 56497545\cos(25\phi_0) + 2414425\cos(27\phi_0)), \tag{A.6i}$$

$$W_{10} = -\frac{I^6}{31310311587840\sqrt{2}(-k)^{15/2}}(45945339825\sin(2\phi_0) - 25307205900\sin(4\phi_0) + 16767524845\sin(6\phi_0) - 10811740260\sin(8\phi_0) + 6456248907\sin(10\phi_0) - 3480781220\sin(12\phi_0) + 1652572455\sin(14\phi_0) - 676366320\sin(16\phi_0) + 233384255\sin(18\phi_0) - 66206628\sin(20\phi_0) + 14975235\sin(22\phi_0) - 2591380\sin(24\phi_0) + 322245\sin(26\phi_0) - 25740\sin(28\phi_0) + 1001\sin(30\phi_0)). \tag{A.6j}$$

Classical functions $\mathcal{O}_1(\phi_0,\ I;\ x)$ and $\mathcal{O}_2(\phi_0,\ I;\ x)$ up to the first order in $\lambda' = \sqrt{\lambda}$ (the complete list can be obtained under request):

$$\mathcal{O}_1 = -\frac{3k}{(\lambda')^2} - \frac{2^{3/4}\sqrt{3}\sqrt[4]{-k}\sqrt{I}}{\lambda'}\sin(\phi_0) + \frac{I}{4\sqrt{2}\sqrt{-k}}(\sin^2(\phi_0) + \sin(\phi_0)\sin(3\phi_0)) + \frac{I^{3/2}\lambda'}{64\ 2^{3/4}\sqrt{3}(-k)^{5/4}}(37\cos(2\phi_0)\sin(\phi_0) - 16\cos(4\phi_0)\sin(\phi_0) + 3\cos(6\phi_0)\sin(\phi_0) + 57\sin^3(\phi_0) - 22\sin^2(\phi_0)\sin(3\phi_0) + \sin(\phi_0)\sin^2(3\phi_0)), \tag{A.7}$$

$$\mathcal{O}_2 = \frac{3k^2}{2(\lambda')^4} - \frac{2^{3/4}\sqrt{3}(-k)^{5/4}\sqrt{I}}{(\lambda')^3}\sin(\phi_0) + \frac{I\sqrt{-k}}{4\sqrt{2}(\lambda')^2}(9\sin^2(\phi_0) + \sin(\phi_0)\sin(3\phi_0))$$
$$+\frac{I^{3/2}}{64\,2^{3/4}\sqrt{3}\sqrt[4]{-k}\lambda'}(37\cos(2\phi_0)\sin(\phi_0)$$
$$-16\cos(4\phi_0)\sin(\phi_0) + 3\cos(6\phi_0)\sin(\phi_0) + 25\sin^3(\phi_0) - 54\sin^2(\phi_0)\sin(3\phi_0) + \sin(\phi_0)\sin^2(3\phi_0))$$
$$+\frac{I^2}{12288(-k)}(-802\sin^2(\phi_0) - 3996\cos(2\phi_0)\sin^2(\phi_0) + 1728\cos(4\phi_0)\sin^2(\phi_0) - 324\cos(6\phi_0)\sin^2(\phi_0)$$
$$-3692\sin^4(\phi_0) + 888\sin(\phi_0)\sin(3\phi_0) + 148\cos(2\phi_0)\sin(\phi_0)\sin(3\phi_0) - 64\cos(4\phi_0)\sin(\phi_0)\sin(3\phi_0)$$
$$+12\cos(6\phi_0)\sin(\phi_0)\sin(3\phi_0) + 1644\sin^3(\phi_0)\sin(3\phi_0) - 36\sin^2(\phi_0)\sin^2(3\phi_0) + 4\sin(\phi_0)\sin^3(3\phi_0)$$
$$-560\sin(\phi_0)\sin(5\phi_0) + 161\sin(\phi_0)\sin(7\phi_0) - 21\sin(\phi_0)\sin(9\phi_0)) + \frac{I^{5/2}\lambda'}{196608\sqrt{3}(-k)^{7/4}}(8672\cos(2\phi_0)\sin(\phi_0)$$
$$+1369\cos^2(2\phi_0)\sin(\phi_0) - 7576\cos(4\phi_0)\sin(\phi_0) - 1184\cos(2\phi_0)\cos(4\phi_0)\sin(\phi_0) + 256\cos^2(4\phi_0)\sin(\phi_0)$$
$$+4752\cos(6\phi_0)\sin(\phi_0) + 222\cos(2\phi_0)\cos(6\phi_0)\sin(\phi_0) - 96\cos(4\phi_0)\cos(6\phi_0)\sin(\phi_0)$$
$$+9\cos^2(6\phi_0)\sin(\phi_0)$$
$$-1856\cos(8\phi_0)\sin(\phi_0) + 400\cos(10\phi_0)\sin(\phi_0) - 40\cos(12\phi_0)\sin(\phi_0) + 21654\sin^3(\phi_0)$$
$$+30414\cos(2\phi_0)\sin^3(\phi_0)$$
$$-13152\cos(4\phi_0)\sin^3(\phi_0) + 2466\cos(6\phi_0)\sin^3(\phi_0) + 5781\sin^5(\phi_0) - 24778\sin^2(\phi_0)\sin(3\phi_0)$$
$$-1332\cos(2\phi_0)\sin^2(\phi_0)\sin(3\phi_0) + 576\cos(4\phi_0)\sin^2(\phi_0)\sin(3\phi_0) - 108\cos(6\phi_0)\sin^2(\phi_0)\sin(3\phi_0)$$
$$-28\sin^4(\phi_0)\sin(3\phi_0) + 888\sin(\phi_0)\sin^2(3\phi_0) + 222\cos(2\phi_0)\sin(\phi_0)\sin^2(3\phi_0)$$
$$-96\cos(4\phi_0)\sin(\phi_0)\sin^2(3\phi_0)$$
$$+18\cos(6\phi_0)\sin(\phi_0)\sin^2(3\phi_0) - 498\sin^3(\phi_0)\sin^2(3\phi_0) - 60\sin^2(\phi_0)\sin^3(3\phi_0) + 5\sin(\phi_0)\sin^4(3\phi_0)$$
$$+15120\sin^2(\phi_0)\sin(5\phi_0) - 560\sin(\phi_0)\sin(3\phi_0)\sin(5\phi_0) - 4347\sin^2(\phi_0)\sin(7\phi_0)$$
$$+161\sin(\phi_0)\sin(3\phi_0)\sin(7\phi_0) + 567\sin^2(\phi_0)\sin(9\phi_0) - 21\sin(\phi_0)\sin(3\phi_0)\sin(9\phi_0)). \tag{A.8}$$

Coefficients $\beta_1^{(n')}(I;x)$ and $\beta_2^{(n')}(I;x)$ for $n' = 0,\ 1,\ \ldots,\ 10$:

$$\beta_1^{(0)} = -\frac{0.707107I}{\sqrt{-k}} - \frac{3k}{(\lambda')^2} - \frac{0.125I^2(\lambda')^2}{k^2} - \frac{0.0521737I^3(\lambda')^4}{(-k)^{7/2}} + \frac{0.0271267I^4(\lambda')^6}{k^5} - \frac{0.0156621I^5(\lambda')^8}{(-k)^{13/2}}$$
$$+\frac{0.00212907I^6(\lambda')^{10}}{k^8}, \tag{A.9a}$$

$$\beta_1^{(1)} = \frac{1.45648\mathrm{i}\sqrt[4]{-k}\sqrt{I}}{\lambda'} - \frac{0.128735\mathrm{i}I^{3/2}\lambda'}{(-k)^{5/4}} - \frac{0.0393514\mathrm{i}I^{5/2}(\lambda')^3}{(-k)^{11/4}} - \frac{0.0185784\mathrm{i}I^{7/2}(\lambda')^5}{(-k)^{17/4}} - \frac{0.0103102\mathrm{i}I^{9/2}(\lambda')^7}{(-k)^{23/4}}$$
$$-\frac{0.00622176\mathrm{i}I^{11/2}(\lambda')^9}{(-k)^{29/4}}, \tag{A.9b}$$

$$\beta_1^{(2)} = -\frac{0.353553I}{\sqrt{-k}} - \frac{0.0520833I^2(\lambda')^2}{k^2} - \frac{0.0191048I^3(\lambda')^4}{(-k)^{7/2}} + \frac{0.00896313I^4(\lambda')^6}{k^5} - \frac{0.00474387I^5(\lambda')^8}{(-1.k)^{13/2}}$$
$$-\frac{0.000633553I^6(\lambda')^{10}}{k^8} \tag{A.9c}$$

$$\beta_1^{(3)} = -\frac{0.0643677\mathrm{i}I^{3/2}\lambda'}{(-k)^{5/4}} - \frac{0.0256021\mathrm{i}I^{5/2}(\lambda')^3}{(-k)^{11/4}} - \frac{0.0130956\mathrm{i}I^{7/2}(\lambda')^5}{(-k)^{17/4}} - \frac{0.00747685\mathrm{i}I^{9/2}(\lambda')^7}{(-k)^{23/4}}$$
$$-\frac{0.00454997\mathrm{i}I^{11/2}(\lambda')^9}{(-k)^{29/4}}, \tag{A.9d}$$

$$\beta_1^{(4)} = \frac{0.0104167I^2(\lambda')^2}{k^2} + \frac{0.00675189I^3(\lambda')^4}{(-k)^{7/2}} - \frac{0.00433124I^4(\lambda')^6}{k^5} + \frac{0.00284286I^5(\lambda')^8}{(-k)^{13/2}} + \frac{0.00230256I^6(\lambda')^{10}}{k^8}, \tag{A.9e}$$

$$\beta_1^{(5)} = \frac{0.00158038\mathrm{i}I^{5/2}(\lambda')^3}{(-k)^{11/4}} + \frac{0.00142015\mathrm{i}I^{7/2}(\lambda')^5}{(-k)^{17/4}} + \frac{0.00109183\mathrm{i}I^{9/2}(\lambda')^7}{(-k)^{23/4}} + \frac{0.000807709\mathrm{i}I^{11/2}(\lambda')^9}{(-k)^{29/4}}, \tag{A.9f}$$

$$\beta_1^{(6)} = -\frac{0.000230178I^3(\lambda')^4}{(-k)^{7/2}} + \frac{0.000264486I^4(\lambda')^6}{k^5} - \frac{0.000236772I^5(\lambda')^8}{(-k)^{13/2}} - \frac{0.000868488I^6(\lambda')^{10}}{k^8} \tag{A.9g}$$

$$\beta_1^{(7)} = -\frac{0.0000325936\mathrm{i}I^{7/2}(\lambda')^5}{(-k)^{17/4}} - \frac{0.0000456142\mathrm{i}I^{9/2}(\lambda')^7}{(-k)^{23/4}} - \frac{0.000046581\mathrm{i}I^{11/2}(\lambda')^9}{(-k)^{29/4}}, \tag{A.9h}$$

$$\beta_1^{(8)} = -\frac{4.521122685185185\times10^{-6}I^4(\lambda')^6}{k^5} + \frac{7.459471854965145\times10^{-6}I^5(\lambda')^8}{(-k)^{13/2}} + \frac{0.000701564I^6(\lambda')^{10}}{k^8}, \tag{A.9i}$$

$$\beta_1^{(9)} = \frac{6.173347113384545\times10^{-7}\mathrm{i}I^{9/2}(\lambda')^7}{(-k)^{23/4}} + \frac{1.1731516942448892\times10^{-6}\mathrm{i}I^{11/2}(\lambda')^9}{(-k)^{29/4}}, \tag{A.9j}$$

$$\beta_1^{(10)} = -\frac{8.325303409559314\times10^{-8}I^5(\lambda')^8}{(-k)^{13/2}} - \frac{0.000568826I^6(\lambda')^{10}}{k^8}, \tag{A.9k}$$

$$\beta_2^{(0)} = \frac{0.125I^2}{k} + \frac{1.5k^2}{(\lambda')^4} - \frac{0.0417389I^3(\lambda')^2}{(-k)^{5/2}} - \frac{0.0203451I^4(\lambda')^4}{k^4} - \frac{0.0113906I^5(\lambda')^6}{(-k)^{11/2}} - \frac{0.00487782I^6(\lambda')^8}{k^7} - \frac{0.000355413I^7(\lambda')^{10}}{(-k)^{17/2}}, \tag{A.10a}$$

$$\beta_2^{(1)} = \frac{1.45648\mathrm{i}(-k)^{5/4}\sqrt{I}}{(\lambda')^3} - \frac{0.300383\mathrm{i}I^{3/2}}{\sqrt[4]{-k}\,\lambda'} - \frac{0.0519944\mathrm{i}I^{5/2}\lambda'}{(-k)^{7/4}} - \frac{0.0225082\mathrm{i}I^{7/2}(\lambda')^3}{(-k)^{13/4}} - \frac{0.0119265\mathrm{i}I^{9/2}(\lambda')^5}{(-k)^{19/4}} - \frac{0.00697415\mathrm{i}I^{11/2}(\lambda')^7}{(-k)^{25/4}} + \frac{0.000365442\mathrm{i}I^{13/2}(\lambda')^9}{(-k)^{31/4}}, \tag{A.10b}$$

$$\beta_2^{(2)} = -\frac{0.0625I^2}{k} - \frac{0.707107\sqrt{-k}\,I}{(\lambda')^2} + \frac{0.0133503I^3(\lambda')^2}{(-k)^{5/2}} + \frac{0.00576443I^4(\lambda')^4}{k^4} + \frac{0.0031454I^5(\lambda')^6}{(-1.k)^{11/2}} - \frac{0.00397671I^6(\lambda')^8}{k^7} + \frac{0.00217812I^7(\lambda')^{10}}{(-k)^{17/2}}, \tag{A.10c}$$

$$\beta_2^{(3)} = -\frac{0.236015\mathrm{i}I^{3/2}}{\sqrt[4]{-k}\,\lambda'} - \frac{0.0256021\mathrm{i}I^{5/2}\lambda'}{(-k)^{7/4}} - \frac{0.00979904\mathrm{i}I^{7/2}(\lambda')^3}{(-k)^{13/4}} - \frac{0.00473918\mathrm{i}I^{9/2}(\lambda')^5}{(-k)^{19/4}} - \frac{0.0025574\mathrm{i}I^{11/2}(\lambda')^7}{(-k)^{25/4}} + \frac{0.000746187\mathrm{i}I^{13/2}(\lambda')^9}{(-k)^{31/4}}, \tag{A.10d}$$

$$\beta_2^{(4)} = -\frac{0.0625I^2}{k} + \frac{0.0208695I^3(\lambda')^2}{(-k)^{5/2}} + \frac{0.0100731I^4(\lambda')^4}{k^4} + \frac{0.0055653I^5(\lambda')^6}{(-k)^{11/2}} - \frac{0.00370461I^6(\lambda')^8}{k^7} + \frac{0.000739686I^7(\lambda')^{10}}{(-k)^{17/2}}, \tag{A.10e}$$

$$\beta_2^{(5)} = \frac{0.0142234\mathrm{i}I^{5/2}\lambda'}{(-k)^{7/4}} + \frac{0.00812512\mathrm{i}I^{7/2}(\lambda')^3}{(-k)^{13/4}} + \frac{0.00488775\mathrm{i}I^{9/2}(\lambda')^5}{(-k)^{19/4}} + \frac{0.00307544\mathrm{i}I^{11/2}(\lambda')^7}{(-k)^{25/4}} + \frac{0.00190357\mathrm{i}I^{13/2}(\lambda')^9}{(-k)^{31/4}}, \tag{A.10f}$$

$$\beta_2^{(6)} = -\frac{0.00291559I^3(\lambda')^2}{(-k)^{5/2}} - \frac{0.00237359I^4(\lambda')^4}{k^4} - \frac{0.00171874I^5(\lambda')^6}{(-k)^{11/2}} + \frac{0.00189226I^6(\lambda')^8}{k^7} - \frac{0.000236153I^7(\lambda')^{10}}{(-k)^{17/2}}, \tag{A.10g}$$

$$\beta_2^{(7)} = -\frac{0.000554091\mathrm{i}I^{7/2}(\lambda')^3}{(-k)^{13/4}} - \frac{0.000587222\mathrm{i}I^{9/2}(\lambda')^5}{(-k)^{19/4}} - \frac{0.000497969\mathrm{i}I^{11/2}(\lambda')^7}{(-k)^{25/4}} - \frac{0.000701971\mathrm{i}I^{13/2}(\lambda')^9}{(-k)^{31/4}}, \tag{A.10h}$$

$$\beta_2^{(8)} = \frac{0.0000994647I^4(\lambda')^4}{k^4} + \frac{0.000130008I^5(\lambda')^6}{(-k)^{11/2}} - \frac{0.000819443I^6(\lambda')^8}{k^7} - \frac{0.000590389I^7(\lambda')^{10}}{(-k)^{17/2}}, \tag{A.10i}$$

$$\beta_2^{(9)} = \frac{0.0000170796\mathrm{i}I^{9/2}(\lambda')^5}{(-k)^{19/4}} + \frac{0.0000265642\mathrm{i}I^{11/2}(\lambda')^7}{(-k)^{25/4}} + \frac{0.000695185\mathrm{i}I^{13/2}(\lambda')^9}{(-k)^{31/4}}, \tag{A.10j}$$

$$\beta_2^{(10)} = -\frac{2.8306031592501667\times10^{-6}I^5(\lambda')^6}{(-k)^{11/2}} + \frac{0.000573754I^6(\lambda')^8}{k^7} + \frac{0.000484516I^7(\lambda')^{10}}{(-k)^{17/2}}. \tag{A.10k}$$

Appendix B. Identification for the action variable

Here, we determine the value of the action variable I and its various powers by using the semiclassical relationship between classical and quantum metrics [22]

$$\hbar^2 g_{ij} = g_{ij}^{\mathrm{cl}}. \tag{B.1}$$

For the metrics components (24) and (34) of the case $k > 0$ we have the relations $\hbar^2 g_{11} = g_{11}^{\mathrm{cl}}$, $\hbar^2 g_{12} = g_{12}^{\mathrm{cl}}$, and $\hbar^2 g_{22} = g_{22}^{\mathrm{cl}}$. For each of these relations, we get an identification of the α-th power of the action variable I as $I^\alpha = (f_\alpha \hbar)^\alpha$ ($\alpha = 1, 2, \ldots, 14$) where f_α are the numerical coefficients. However, using (24) and (34) the values obtained for f_α from each relation are slightly different. Then, we take as the value of f_α the average value of the resulting values, obtaining $f_1 = 0.5, f_2 = 1, f_3 = 1.1447, f_4 = 1.2484, f_5 = 1.3372, f_6 = 1.4186, f_7 = 1.4962, f_8 = 1.5720, f_9 = 1.6470, f_{10} = 1.7219, f_{11} = 1.7972, f_{12} = 1.8730, f_{13} = 1.9433$, and $f_{14} = 2.0120$. In figure B1, we show f_α as a function of α.

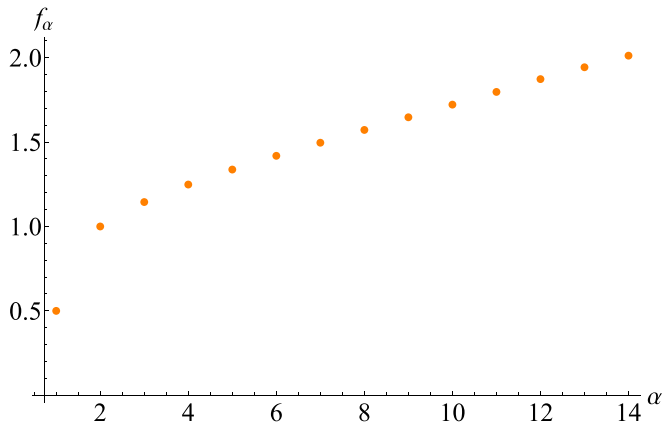

Figure B1. Coefficients f_α of the identifications as a function α.

Appendix C. Comparison of differences of energies

Comparing the quantum metric (3) and the classic metric (13), suggests that exact excitation energies, $E_m - E_0$, have a counterpart in the classical approximation given by the harmonic oscillator energies $m'\omega$. In figure C1(a) we plot $E_m - E_0$ and $m'\omega$ for $k = 1$ and $\lambda = 0.2$, finding that for small values of m and m' ($m,\ m' < 10$), the quantities $E_m - E_0$ and $m'\omega$ remain close to each other. However, for large values of m and m' ($m,\ m' > 10$), $E_m - E_0$ deviates from the linear behavior of $m'\omega$, which is a consequence of quantum corrections. On the other hand, in table C1 are shown the first seven values of the energies for the case $k = -1$ and $\lambda = 0.2$. From this it is clear that $E_m \approx E_{m+1}$ for even m, which is a quasi-degeneration that emerges as a consequence of the double well potential. In contrast, in the classical case, all 'excitation' energies $m'\omega$ appear only once. This is because, in the classical perturbation formalism for the case $k < 0$, we have considered only one of the wells, the one associated with the fixed point χ_1. It can be verified that employing the well involving the fixed point χ_2, the

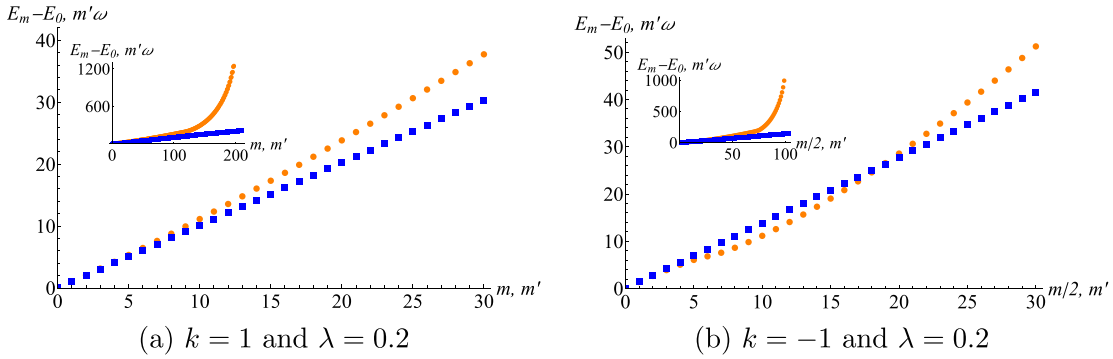

Figure C1. Comparison between $E_m - E_0$ and $m'\omega$. Orange round markers correspond to $E_m - E_0$ and blue square markers correspond to $m'\omega$.

Table C1. Energies in the case $k = -1$ and $\lambda = 0.2$.

n	E_n
0	0
1	1.04×10^{-11}
2	1.360 866
3	1.360 866
4	2.661 983
5	2.661 984
6	3.893 522
7	3.893 550

resulting CMT for $k < 0$ is again (41). In figure C1(b) we plot $E_m - E_0$ and $m'\omega$ as functions of $m/2$ and m', respectively. We can see that both quantities present a similar behavior for small values of m ($m/2 < 20$) and m' ($m' < 20$).

ORCID iDs

Diego Gonzalez https://orcid.org/0000-0002-0206-7378
Jorge Chávez-Carlos https://orcid.org/0000-0002-5223-5931
Jorge G Hirsch https://orcid.org/0000-0002-2170-9903
J David Vergara https://orcid.org/0000-0002-8615-761X

References

[1] Provost J P and Vallee G 1980 *Commun. Math. Phys.* **76** 289–301
[2] Zanardi P, Giorda P and Cozzini M 2007 *Phys. Rev. Lett.* **99** 100603
[3] Kumar P, Mahapatra S, Phukon P and Sarkar T 2012 *Phys. Rev.* E **86** 051117
[4] Gu S J 2010 *Int. J. of Mod. Phys.* B **24** 4371–458
[5] Carollo A, Valenti D and Spagnolo B 2020 *Phys. Rep.* **838** 1–72
[6] Zanardi P and Rasetti M 1999 *Phys. Lett.* A **264** 94–9
[7] Rezakhani A T, Abasto D F, Lidar D A and Zanardi P 2010 *Phys. Rev.* A **82** 012321
[8] Ozawa T and Goldman N 2018 *Phys. Rev.* B **97** 201117(R)
[9] Ozawa T and Goldman N 2019 *Physical Review Research* **1** 032019
[10] Tan X *et al* 2019 *Phys. Rev. Lett.* **122** 210401
[11] Yu M *et al* 2019 *Natl Sci. Rev.* **7** 254–60
[12] Li C, Chen M and Cappellaro P 2022 A geometric perspective: experimental evaluation of the quantum cramer-rao bound arXiv:2204.13777
[13] Min Y *et al* 2022 *npj Quantum Information* **8** 56
[14] Okun P and Burke K 2021 *Int. J. Quantum Chem.* **121** e26554
[15] Turbiner A V 1984 *Sov. Phys. Usp.* **27** 668–94
[16] Alvarez-Jimenez J, Dector A and Vergara J D 2017 *J. High Energy Phys.* **2017** 044
[17] Campos Venuti L and Zanardi P 2007 *Phys. Rev. Lett.* **99** 095701
[18] Tully J C 1990 *J. Chem. Phys.* **93** 1061–71
[19] Hetényi B and Lévay P 2023 *Phys. Rev.* A **108** 032218
[20] Sokolnikoff I 1951 *Tensor Analysis: Theory and Applications* Applied mathematics series (Wiley)
[21] Gonzalez D, Gutiérrez-Ruiz D and Vergara J D 2019 *Phys. Rev.* E **99** 032144
[22] Alvarez-Jimenez J, Gonzalez D, Gutiérrez-Ruiz D and Vergara J D 2020 *Ann. Phys. (Berlin)* **532** 1900215
[23] Gonzalez D, Gutiérrez-Ruiz D, Vergara J D and Hernandez M J 2024 *Work in preparation*
[24] Bender C M and Wu T T 1969 *Phys. Rev.* **184** 1231–60
[25] Bender C M and Wu T T 1973 *Phys. Rev.* D **7** 1620–36
[26] Lipatov L N 1977 *Sov. Phys. JETP* **45** 216–23
[27] Brézin E, Le Guillou J C and Zinn-Justin J 1977 *Phys. Rev.* D **15** 1544–57
[28] Seznec R and Zinn-Justin J 2008 *J. Math. Phys.* **20** 1398–408
[29] Zinn-Justin J 1981 *J. Math. Phys.* **22** 511–20
[30] Zinn-Justin J 1981 *Phys. Rep.* **70** 109–67
[31] Zinn-Justin J 2010 *Path Integrals in Quantum Mechanics* (Oxford, United Kingdom: Oxford University Press) (https://books.google.com.mx/books?id=bc2xQwAACAAJ)
[32] Zinn-Justin J 1981 *Nucl. Phys.* B **192** 125–40
[33] Zinn-Justin J 1983 *Nucl. Phys.* B **218** 333–48
[34] Caswell W E 1979 *Ann. Phys.* **123** 153–84
[35] Turbiner A 2005 *Lett. Math. Phys.* **74** 169–80
[36] Jentschura U D and Zinn-Justin J 2010 *Appl. Numer. Math.* **60** 1332–41 ISSN 0168-9274 approximation and extrapolation of convergent and divergent sequences and series (CIRM, Luminy—France, 2009)
[37] Turbiner A V and del Valle J C 2021 *J. Phys. A: Math. Theor.* **54** 295204
[38] Turbiner A V and del Valle J C 2022 *Acta Polytechnica* **62** 208–10
[39] Nader D J, Hernandez-Gonzalez J R, Vazquez-Sanchez H and Lerma-Hernandez S 2023 *Manifestation of instability in the quasiclassical limit of the spectrum of the quartic double well* arXiv:2302.14211
[40] Inc W R Mathematica, Version 13.2 Champaign, IL, 2022 https://www.wolfram.com/mathematica
[41] Dittrich W and Reuter M 2020 *Classical and Quantum Dynamics* (Cham, Switzerland: Springer)
[42] Goldstein H, Poole C and Safko J 2000 *Classical Mechanics* 3rd ed (Addison Wesley)
[43] Gutiérrez-Ruiz D, Gonzalez D, Chávez-Carlos J, Hirsch J G and Vergara J D 2021 *Phys. Rev.* B **103** 174104
[44] Yuce C, Kilic A and Coruh A 2006 *Phys. Scr.* **74** 114
[45] Ali T, Bhattacharyya A, Haque S S, Kim E H, Moynihan N and Murugan J 2020 *Phys. Rev.* D **101** 026021
[46] Crespo-Otero R and Barbatti M 2018 *Chem. Rev.* **118** 7026–68